Acta Crystallographica Section D
Biological Crystallography
ISSN 1399-0047

Structures of inactive CRP species reveal the atomic details of the allosteric transition that discriminates cyclic nucleotide second messengers

Seung-Hyeon Seok,[a]‡ Hookang Im,[a]‡ Hyung-Sik Won,[b]‡ Min-Duk Seo,[c,d] Yoo-Sup Lee,[b] Hye-Jin Yoon,[e] Min-Jeong Cha,[a] Jin-Young Park[a] and Bong-Jin Lee[a]*

[a]Research Institute of Pharmaceutical Sciences, College of Pharmacy, Seoul National University, Seoul 151-742, Republic of Korea, [b]Department of Biotechnology, RIBHS and RIID, College of Biomedical and Health Science, Konkuk University, Chungju, Chungbuk 380-701, Republic of Korea, [c]College of Pharmacy, Ajou University, Suwon, Kyeonggi 443-749, Republic of Korea, [d]Department of Molecular Science and Technology, Ajou University, Suwon, Kyeonggi 443-749, Republic of Korea, and [e]Department of Chemistry, College of Natural Sciences, Seoul National University, Seoul 151-742, Republic of Korea

‡ These authors contributed equally to this work.

Correspondence e-mail: lbj@nmr.snu.ac.kr

Received 3 December 2013
Accepted 1 April 2014

PDB references: CRP, 4n9h; cGMP complex, 4n9i

The prokaryotic global transcription factor CRP has been considered to be an ideal model for in-depth study of both the allostery of the protein and the differential utilization of the homologous cyclic nucleotide second messengers cAMP and cGMP. Here, atomic details from the crystal structures of two inactive CRP species, an apo form and a cGMP-bound form, in comparison with a known active conformation, the cAMP–CRP complex, provide macroscopic and microscopic insights into CRP allostery, which is coupled to specific discrimination between the two effectors. The cAMP-induced conformational transition, including dynamic fluctuations, can be driven by the fundamental folding forces that cause water-soluble globular proteins to construct an optimized hydrophobic core, including secondary-structure formation. The observed conformational asymmetries underlie a negative cooperativity in the sequential binding of cyclic nucleotides and a stepwise manner of binding with discrimination between the effector molecules. Additionally, the finding that cGMP, which is specifically recognized in a *syn* conformation, induces an inhibitory conformational change, rather than a null effect, on CRP supports the intriguing possibility that cGMP signalling could be widely utilized in prokaryotes, including in aggressive inhibition of CRP-like proteins.

1. Introduction

Cyclic nucleotide second messengers, particularly cyclic adenosine 3′,5′-monophosphate (cAMP) and cyclic guanosine 3′,5′-monophosphate (cGMP), are appreciated to be key regulatory elements of living organisms that mediate cellular responses to stimuli (Rehmann *et al.*, 2007; Das *et al.*, 2009; Gomelsky, 2011). The receptor proteins for these molecules in eukaryotes include protein kinase A (PKA), protein kinase G (PKG), the Rap guanine nucleotide-exchange factor Epac and cyclic nucleotide-regulated ion channels (Rehmann *et al.*, 2007). As an exemplar of the second-messenger concept, cAMP signals have been well elucidated in prokaryotes (You *et al.*, 2013; Botsford & Harman, 1992) and in eukaryotes. Subsequently, the cAMP receptor protein (CRP) from *Escherichia coli* has provided the first insights into the structural basis of cAMP action (Rehmann *et al.*, 2007). Conversely, the involvement of cGMP in bacterial signalling has been controversial; however, recent advances in studies on cGMP and guanylate cyclases have confirmed such a role for cGMP, which has led to renewed interest (Gomelsky & Galperin, 2013; Gomelsky, 2011; Linder, 2010). In this respect, CRP, as one of the most ancient receptors of cyclic nucleoside monophosphates (cNMPs), has also been considered to be a key

molecule to address the structural and evolutionary enigma of how similar cNMPs such as cAMP and cGMP can be adapted to control diverse and specific processes (Gomelsky, 2011). Additionally, CRP has long served as a typical textbook example for transcriptional regulation, DNA-binding motifs and allosteric activation of a protein (Won *et al.*, 2009; Harman, 2001). Upon binding of the effector molecule cAMP, activated CRP binds to target DNA sites that are located in or adjacent to promoter regions. CRP binding to DNA results in DNA bending and the concomitant recruitment of RNA polymerase (RNAP) to initiate gene transcription. Because the concentration of cAMP increases upon the reduction of glucose levels in *E. coli*, the primary targets of the cAMP–CRP paradigm are catabolite genes. Thus, CRP is also referred to as CAP (catabolite gene-activator protein), but the gene encoding this protein has been given the official name *crp*. Indeed, CRP, as the sensor of cAMP levels in cells, is regarded as a prokaryotic global transcription regulator that controls the expression of nearly 200 genes and is not restricted to catabolite genes (Hollands *et al.*, 2007).

CRP is a homodimeric protein, with each subunit consisting of a C-terminal DNA-binding domain (CDD), an N-terminal nucleotide-binding domain (NND) and a short flexible stretch that connects the two domains, referred to as the interdomain 'hinge' region. In particular, the C-terminal F-helix (αF) of CRP, which forms a canonical helix–turn–helix motif with the neighbouring E-helix (αE), is responsible for specific DNA recognition. However, the protein does not operate in the absence of bound cAMP, although the binding site is located apart from the DNA-binding region. Thus, the cAMP-induced activation process of CRP for DNA binding is a classic example of allosteric conformational change (Won *et al.*, 2009; Harman, 2001). In addition, recent advances in protein dynamics have contributed to an understanding of its dynamic allostery (Tzeng & Kalodimos, 2009, 2012; Popovych *et al.*, 2006). However, understanding the structural basis of the transition is essential for thorough elucidation of CRP allostery, and this necessarily requires atomic details of the inactive-state and active-state conformations. In this context, the greater than ten three-dimensional structures that are available in the Protein Data Bank provide full pictures of the active-state CRP conformation (Won *et al.*, 2009), including the CRP–cAMP, CRP–cAMP–DNA and CRP–cAMP–DNA–RNAP complexes and some constitutively active mutant forms of CRP, namely CRP* mutants. Unfortunately, however, the conformational aspects of the allosteric transition still remain controversial owing to conflicting reports regarding the inactive conformation. Concretely, the ligand-free apo CRP structure has been independently solved using X-ray crystallography (Sharma *et al.*, 2009), albeit at low resolution (3.6 Å) and with a mutant (D138L) form of the protein, and by NMR in solution (Popovych *et al.*, 2009). However, the NMR and crystal structures were distinct from each other, thereby supporting conflicting models of the conformational allostery.

In the present study, we succeeded in obtaining a higher resolution (2.2 Å) crystal structure of wild-type apo CRP, which would be the most suitable template for the precise inspection of the inactive conformation in order to establish the mode of conformational transition in atomic detail. In addition, we report the first crystal structure of another inactive form, the cGMP–CRP complex, also at 2.2 Å resolution, which underpins our insight into its conformational allostery and addresses how CRP discriminates the false ligand cGMP from the *bona fide* effector cAMP and the molecular-evolutionary implications of the discriminating principles. In addition, the emerging insights into the dynamic allostery of CRP are interpreted on the basis of the model for conformational allostery.

2. Materials and methods

2.1. Cloning and protein preparation

Full-length *E. coli* CRP, which was used for the crystallization of the cGMP–CRP complex, was prepared using the recombinant pT7-CRP plasmid as described previously (Won *et al.*, 2000, 2002). For the crystallization of apo CRP containing an N-terminal eight-residue deletion, DNA fragments encoding Pro9–Arg209 were amplified using pT7-CRP as the template and the following pairs of oligonucleotide primers (*Nde*I and *Xho*I restriction sites are shown in bold): the forward primer 5′-G GAA TTC **CAT ATG** CCG ACT CTC GAA TGG TTC-3′ and the reverse primer 5′-CCG CCG **CTC GAG** TTA ACG AGT GCC GTA AAC GAC-3′, which contained a stop codon to produce the protein without artificial histidine tags. The PCR products were purified, digested with *Nde*I and *Xho*I enzymes (NEB) and ligated into an *Nde*I/*Xho*I-digested pET-21a(+) (Novagen) expression vector. Site-directed mutations of CRP at positions 83 and 130 were introduced using the EZchange Site-Directed Mutagenesis Kit (Enzynomics). The primers used were 5′-GC CAG GAA CGT **GCC** GCA TGG GTA CGT-3′ for the S83A mutation and 5′-A GTC ACT TCA GAG **GCA** GTG GGC AAC CT-3′ for the K130A mutation (the mutation sites are shown in bold). *E. coli* BL21(DE3) (Novagen) cells transformed with the constructed plasmids were grown at 37°C in Luria Broth (LB) medium including 100 µg ml^{-1} ampicillin. Protein expression was induced at an OD_{600} of approximately 0.5 by adding isopropyl β-D-1-thiogalactopyranoside (IPTG) to a final concentration of 0.5 m*M* and induction was continued for a further 4 h. To prepare selenomethionine-labelled CRP(9–209) [SeMet-CRP(9–209)], the cells were grown at 25°C in M9 medium containing 100 mg l^{-1} Lys, Phe and Thr, 50 mg l^{-1} Ile, Leu and Val and 60 mg l^{-1} selenomethionine until an OD_{600} of 0.5 was reached (Van Duyne *et al.*, 1993). Protein expression was induced using IPTG, and the cultures were incubated for 12 h. The cells were harvested by centrifugation and disrupted by sonication. After centrifugation, the supernatant was loaded onto a Bio-Rex 70 (Hercules) cation-exchange column. The protein was eluted with a linear gradient from 0 to 1 *M* NaCl in 50 m*M* potassium phosphate buffer containing 1 m*M* EDTA at pH 6.7. Fractions containing CRP were pooled and concentrated to approximately 2 ml by ultrafiltration using an Amicon Ultra (Millipore). The concentrated sample was

Table 1
Data-collection and refinement statistics.

Values in parentheses are for the highest resolution shell.

	Apo CRP	cGMP–CRP
Data collection		
Beamline	PF-AR NW12A	PF-AR NW12A
Wavelength (Å)	0.97922	1.00000
Space group	$P6_1$	$P2_1$
Unit-cell parameters		
a (Å)	120.617	42.568
b (Å)	120.617	56.171
c (Å)	60.349	186.718
α (°)	90	90
β (°)	90	90.18
γ (°)	120	90
Resolution (Å)	50–2.2 (2.24–2.20)	50–2.2 (2.28–2.20)
$R_{\rm merge}$† (%)	8.6 (39.4)	6.6 (14.7)
$\langle I/\sigma(I)\rangle$	94.4 (12.3)	32.8 (12.7)
Multiplicity‡	22.5 (21.9)	6.9 (6.9)
Completeness (%)	99.7 (100)	99.5 (100)
Unique reflections	25544 (1262)	45063 (4489)
Refinement		
$R_{\rm work}$§ (%)	20.2	17.0
$R_{\rm free}$¶ (%)	26.3	20.8
No. of atoms		
Total	3269	6752
Protein	3156	6392
Water	113	268
Ligand	—	92
B factors (Å^2)		
Protein	50.26	33.80
Water	52.85	36.78
R.m.s.d.††		
Bond lengths (Å)	0.019	0.026
Bond angles (°)	2.432	2.116
MolProbity‡‡ (%)	2.59 [44th percentile]	2.17 [75th percentile]
Ramachandran plot (%)		
Preferred region	95.75	95.50
Allowed region	4.00	4.13
Disallowed region	0.25	0.37
PDB code	4n9h	4n9i

† $R_{\rm merge} = \sum_{hkl}\sum_i |I_i(hkl) - \langle I(hkl)\rangle|/\sum_{hkl}\sum_i I_i(hkl)$. ‡ $N_{\rm obs}/N_{\rm unique}$. § $R_{\rm work} = \sum_{hkl} ||F_{\rm obs}| - |F_{\rm calc}||/\sum_{hkl}|F_{\rm obs}|$. ¶ $R_{\rm free}$ was calculated in the same way as $R_{\rm work}$ but using 5% of the reflections which were excluded from the refinement. †† Root-mean-square deviations (r.m.s.d.s) were calculated with *REFMAC*. ‡‡ *MolProbity* analysis (Chen *et al.*, 2010).

applied onto a Superdex 75 (GE Healthcare Biosciences) size-exclusion column that had been equilibrated with the final buffer (20 m*M* Tris pH 7.2, 150 m*M* NaCl, 1 m*M* EDTA). The purified protein was concentrated to approximately 10 mg ml^{-1} in the final buffer. For the crystallization of cGMP–CRP, the protein solution contained 10 m*M* cGMP.

2.2. Crystallization and data collection

Crystals were grown by the hanging-drop vapour-diffusion method at 20°C after mixing equal volumes (2 µl) of protein solution (10 mg ml^{-1} in the final buffer) and reservoir solution. Diffraction-quality apo CRP(9–209) crystals were produced in 3–6 d under the optimal condition 30%(*w*/*v*) polyethylene glycol (PEG) 400, 100 m*M* CHES pH 7.5. Using these conditions, crystals of SeMet-CRP(9–209) could also be produced. Well diffracting crystals of the cGMP–CRP complex appeared in 10–12 d under the condition 22%(*w*/*v*) PEG 8000, 15.4%(*v*/*v*) glycerol, 100 m*M* proline, 50 m*M* HEPES, 88 m*M* potassium phosphate pH 6.4. Prior to data collection, single crystals were equilibrated in the crystallization solution containing an additional 5% glycerol and flash-cooled in liquid nitrogen. Diffraction data for the SeMet-CRP(9–209) and cGMP–CRP crystals were collected using an ADSC Quantum 210 CCD detector on the AR-NW12A beamline at the Photon Factory (PF), Tsukuba, Japan. The data sets were processed and scaled using *HKL*-2000 (Otwinowski & Minor, 1997). The crystals of SeMet-CRP(9–209) and cGMP–CRP belonged to space groups $P6_1$ and $P2_1$, respectively (Table 1).

2.3. Structure determination and refinement

The apo CRP structure was first modelled by MR-SAD (molecular replacement with single anomalous dispersion) using *PHENIX* (Adams *et al.*, 2002). The N-terminal domain (residues 9–130) of the cAMP-bound CRP structure (PDB entry 1g6n; Passner *et al.*, 2000) was used as a search model for molecular replacement. The Matthews coefficient ($V_{\rm M}$; Matthews, 1968) was calculated to be 2.64 Å^3 Da^{-1} (50.6% solvent content) assuming the presence of two molecules in the asymmetric unit. Together with molecular replacement, SAD phasing was performed using *AutoSol* in *PHENIX*, with the anomalous coefficients $f' = 8$ and $f'' = 2$. The phases were further improved by density modification and the model was initially refined using *AutoBuild* in *PHENIX*. The model was then further improved by interactive modelling using *Coot* (Emsley *et al.*, 2010) and was finally refined using *REFMAC* (Murshudov *et al.*, 2011) in the *CCP*4 suite (Winn *et al.*, 2011). $R_{\rm free}$ was calculated by randomly setting aside 5% of the data (Brünger, 1992). After iterative refinement, R and $R_{\rm free}$ reached 20.2 and 26.3%, respectively. To determine the cGMP–CRP structure, molecular replacement was initially performed using the data set with 75% completeness (data not shown) and the N-terminal domain (residues 8–130) of the low-resolution apo CRP structure (PDB entry 3hif; Sharma *et al.*, 2009) as the initial search model. The Matthews coefficient was 2.39 Å^3 Da^{-1} (48.6% solvent content) with four molecules in the asymmetric unit. Refinement was performed using *Coot* and *REFMAC* in the *CCP*4 suite, including bulk-solvent correction. The bound cGMP was included at the final stage of refinement, and R and $R_{\rm free}$ reached 19.2 and 25.0%, respectively. Subsequently, the N-terminal domain of the refined structure was alternatively used as a search model for the new cGMP–CRP data set with higher completeness for improved structure determination (Table 1). Model building and refinement was iteratively performed, and the cGMP molecule was included in the positive electron density during the final refinement. The coordinate file for cGMP was obtained from the *HIC-Up* server (Kleywegt & Jones, 1998), whereas the library for *REFMAC* was generated using the *PRODRG* server (Schüttelkopf & van Aalten, 2004). Finally, the structure was refined to final R and $R_{\rm free}$ values of 17.0 and 20.8%, respectively (Table 1). The atomic coordinates for apo CRP and cGMP–CRP have been deposited in the Protein Data Bank under accession codes 4n9h and 4n9i, respectively.

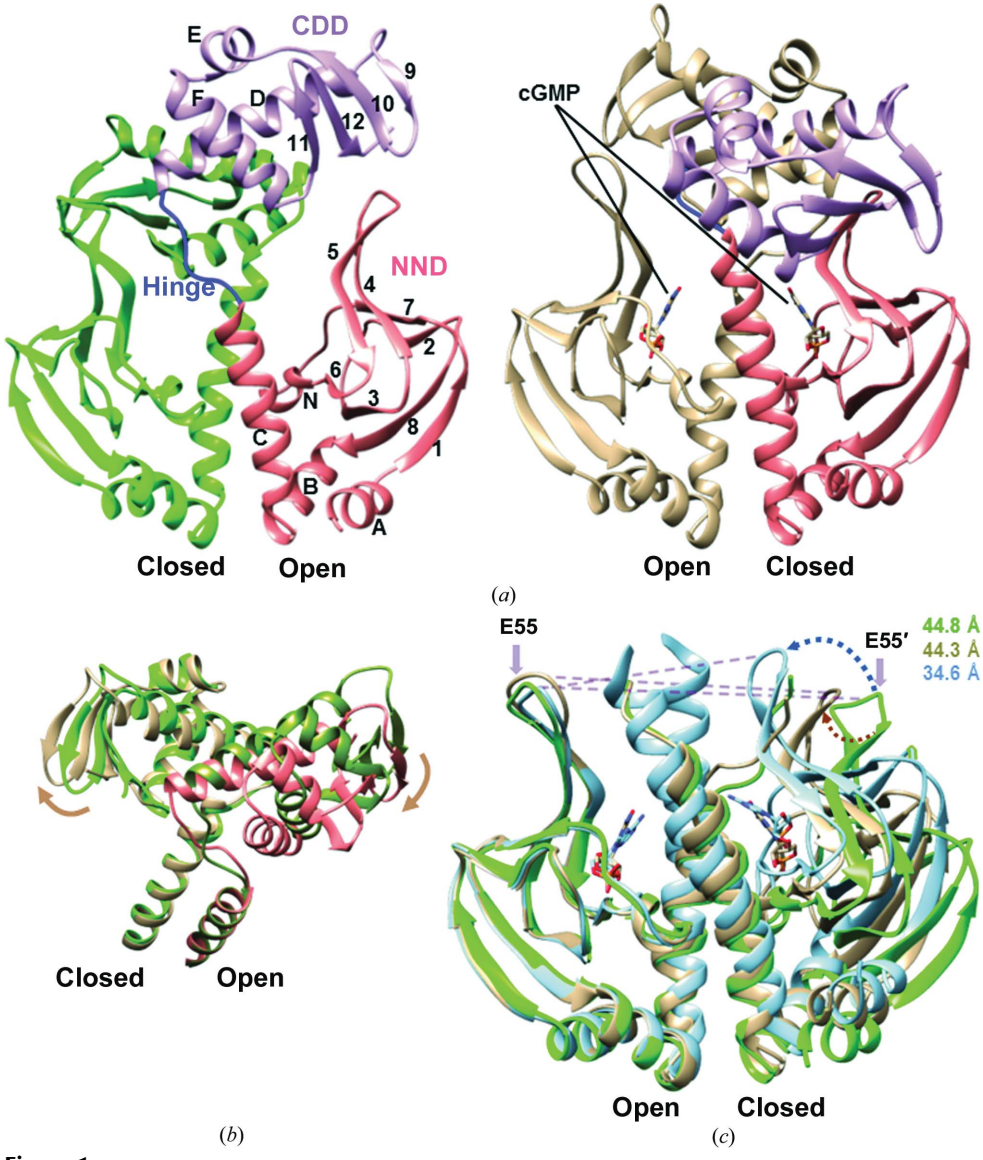

Figure 1
Comparison of the overall conformation between apo CRP and cGMP–CRP. (*a*) The N-terminal nucleotide-binding domain (NND; coloured salmon), the hinge (blue) and the C-terminal DNA-binding domain (CDD; orchid) are indicated in the open subunit of apo CRP (left) and in the closed subunit of cGMP–CRP (right). The closed subunit of apo CRP and the open subunit of cGMP–CRP are coloured green and tan, respectively. Secondary-structure elements are indicated in the open subunit of apo CRP with numbers for β-strands and letters for α-helices and the 3_{10}-helix (ηN). (*b*) The CDD dimers of apo CRP (green and forest green) and cGMP–CRP (salmon and tan) upon superposition of equivalent C^{α} atoms in the αC helix (Asp111–Val126) of the open subunit. A rigid-body rotation of the CDD dimer upon cGMP binding is indicated by arrows. (*c*) The NND dimers of apo CRP (green), cGMP–CRP (tan) and cAMP–CRP (sky blue) upon superposition of equivalent C^{α} atoms in the Thr10–Asn109 region (which precedes αC) of the open subunit. Distances between the flap centres (C^{α} of Glu55) are included for each molecule.

All structural figures were rendered using *UCSF Chimera* (Pettersen *et al.*, 2004).

2.4. Isothermal titration calorimetry

The cGMP binding of wild-type CRP and its S83A and K130A mutants was monitored using a MicroCal Auto-iTC200 calorimeter (GE Healthcare Biosciences) at the Korea Basic Science Institute (Ochang, Republic of Korea). Titrations were carried out at 298 K in assay buffer consisting of 20 m*M* Tris–HCl pH 7.2, 150 m*M* NaCl, 1 m*M* EDTA. All solutions were filtered and thoroughly degassed before use and the concentrations of the protein and cGMP were determined spectrophotometrically using known extinction coefficients (Won *et al.*, 2000, 2002). The concentration of protein in the reaction cell (200 µl) was 78 µ*M* and that of cGMP in the syringe (40 µl) was 2.5 m*M*. A titration experiment consisted of 20 injections. The first injection was 0.4 µl and the subsequent 19 injections were 2 µl each, with an injection interval of 150 s. The obtained heat signals were analysed using the commercial software package (*Origin*) provided by the manufacturer and the data fitting was based on a single-site binding model.

3. Results

3.1. Crystallization of apo CRP and secondary-structure validation

The N-terminus of CRP was reported to be disordered and to not be involved in the functional regulation or structural transition (Won *et al.*, 2000; Sharma *et al.*, 2009; Popovych *et al.*, 2009). Thus, we obtained a high-quality crystal of apo CRP with an improved resolution of up to 2.2 Å (Supplementary Table S1[1]) by deleting the first eight N-terminal residues (Val1–Asp8), which otherwise might be unfavourable for compact crystal packing. The crystals contained one dimer in the asymmetric unit and all regions were clearly refined except for Gln170 and the C-terminus (Thr208 and Arg209), for which only the main chains were traced. For convenience in the comparison, the strand numbers and helix letters in Fig. 1(*a*) were assigned to match the nomenclature that was previously used in the cAMP-bound CRP structure (Passner *et al.*, 2000; Weber & Steitz, 1987). The β2 (residues Thr28–Ile30)

[1] Supporting information has been deposited in the IUCr electronic archive (Reference: MV5099).

and β7 (Asp68–Ile70) strands, which form interstrand hydrogen bonds with the antiparallel β7 and β3 strands, respectively, were also regarded as β-strands, as previously denoted in the cAMP–CRP structure (Passner *et al.*, 2000; Weber & Steitz, 1987), although they are not designated as regular β-strands by the standard *DSSP* criteria (Kabsch & Sander, 1983).

At the level of the secondary structure, the present apo CRP structure exhibited three distinct regions compared with cAMP–CRP. Firstly, the additional helix in the NND, which was not identified in the cAMP–CRP structure (Passner *et al.*, 2000; Weber & Steitz, 1987), was designated ηN (Fig. 1*a*). Our previous NMR analysis (Won *et al.*, 2000) predicted a short helical conformation around Glu72 in apo CRP, which directly interacts with cAMP. The short α-helix at the equivalent position is conserved in other cNMP-binding proteins (Altieri *et al.*, 2008; Berman *et al.*, 2005; Kim *et al.*, 2001; Zhang *et al.*, 2012; Zagotta *et al.*, 2003; Clayton *et al.*, 2004; Schünke *et al.*, 2011; Kumar *et al.*, 2010; Puljung & Zagotta, 2013) and is also observed in *Mycobacterium tuberculosis* CRP (Kumar *et al.*, 2010; Reddy *et al.*, 2009; Gallagher *et al.*, 2009). In the present crystal structure, the presence of a tightly ordered 3_{10}-helix encompassing residues Gly71–Phe76 is evident in both subunits of apo CRP, with consecutive CO(i)–HN(i + 3) hydrogen bonds (Supplementary Fig. S1*a*). Additionally, the ηN helix was also detected in the crystal structure of D138L-CRP (Sharma *et al.*, 2009) and in an NMR structure of apo CRP (Popovych *et al.*, 2009), but it exhibited a relatively loosened conformation owing to fewer hydrogen bonds and/or interference by CO(i)–HN(i + 4) interactions (Supplementary Fig. S1*a*). Subsequently, the ηN helix is not stabilized in the cAMP–CRP complex owing to an insufficient number of tight hydrogen bonds (Supplementary Fig. S1*a*), which is attributable to a slight perturbation in the backbone geometry that is caused by cAMP binding.

The D-helix (αD) in the known NMR structure of apo CRP (Popovych *et al.*, 2009) begins at Thr140, which is consistent with the cAMP-bound crystal structure of CRP (Passner *et al.*, 2000; Weber & Steitz, 1987). However, this finding conflicted with our previous NMR analysis of apo CRP, which predicted Leu134 as the N-terminal residue of αD (Won *et al.*, 2000). The present crystal structure confirms that the αD helix of apo CRP includes Leu134–Lys152, which is consistent with the D138L-CRP crystal structure (Sharma *et al.*, 2009) and our previous NMR analysis (Won *et al.*, 2000). A long αD helix in the apo form has also been suggested from the structure of the CRP-family protein CooA (Lanzilotta *et al.*, 2000; Chan, 2000). The significance of the length of αD for the dimerization of the CDDs is discussed further below.

The most distinctive feature of the present apo CRP structure is the heterogeneity in the lengths observed for the C-helices (αCs), which encompass Asp111–Val126 in one subunit (chain *A*; open subunit) and is further lengthened up to Lys130 in the other subunit (chain *B*; closed subunit). The shorter αC is consistent with that determined by NMR in solution (Popovych *et al.*, 2009; Won *et al.*, 2000), whereas the longer αC is in good agreement with that observed in the D138L-CRP crystal structure (Sharma *et al.*, 2009). However, further examination revealed that the αCs are stabilized as a regular α-helix up to Gln125 in the open subunit, whereas they are elongated up to Glu129 in the closed subunit (Supplementary Fig. S1*b*). The upper regions, *i.e.* Gln125–Glu129 of the open subunit and Glu129–Val131 of the closed subunit, adopt a helical loop conformation that resembles a 3_{10}-helix.

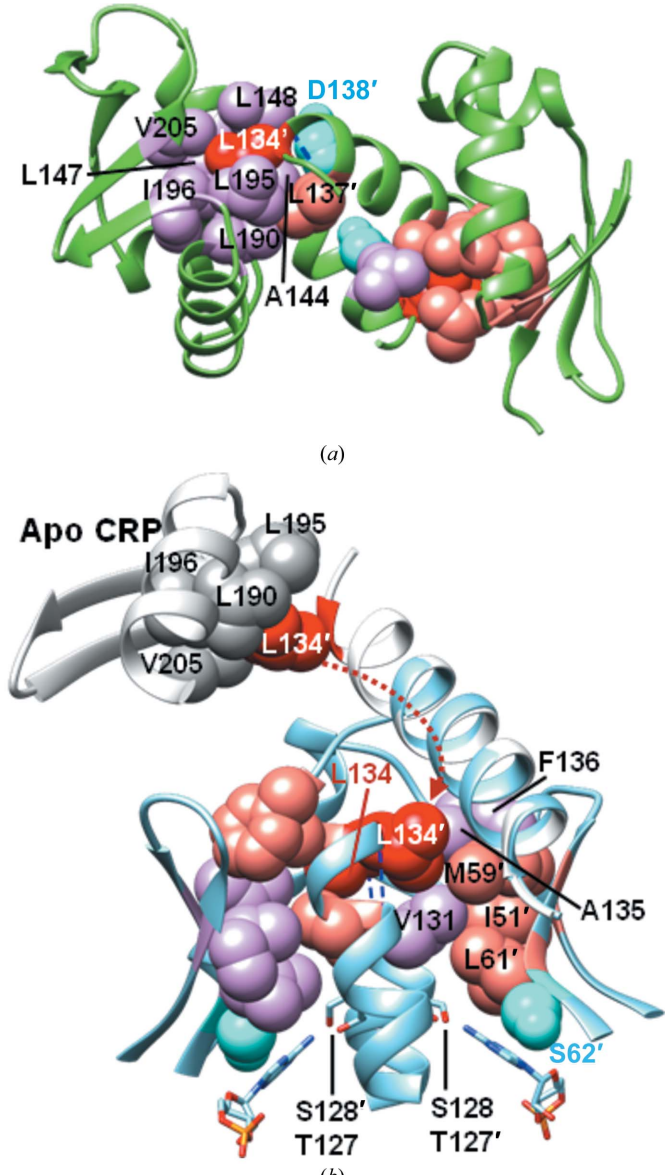

Figure 2
Differences in the Leu134-mediated hydrophobic clusters between apo CRP (*a*) and cAMP–CRP (*b*). The residues in the closed subunit are labelled with primes. Hydrophobic side chains are depicted as spheres and are coloured orchid in the open subunit and salmon in the closed subunit, with the Leu134 residues coloured red. The Asp138 and Ser62 residues that are adjacent to the hydrophobic clusters are shown as cyan spheres. The Leu134-mediated backbone hydrogen bonds are indicated by blue dashed lines. (*a*) The Leu134 residues occupy the centres of the intersubunit hydrophobic clusters that stabilize the CDD dimer in apo CRP. (*b*) Capture of Leu134, which was formerly located in the hydrophobic cluster of the CDD dimer in apo CRP (light grey), in the hydrophobic interface of the NND dimer, as depicted by a dashed red arrow. The bound cAMPs are depicted as sticks with heteroatoms coloured blue for N atoms, red for O atoms and orange for P atoms.

Subsequently, they commonly fold into a portion of a regular α-helix up to Phe136 in the cAMP–CRP complex. Collectively, the interdomain hinge region of apo CRP is defined as Val126–Asn133, and it is suggested that the helical conformation in the Val126–Lys130 region of apo CRP would be transiently adopted or dynamically equilibrated, considering the flexible nature of the hinge (Popovych *et al.*, 2006, 2009; Tomlinson *et al.*, 2006; Lanzilotta *et al.*, 2000). The significance of the hinge conformation for the overall asymmetry of apo CRP is discussed further below.

3.2. C-terminal dimerization of the apo CRP structure

Consistent with what was previously noted in the low-resolution crystal structure of apo CRP (Sharma *et al.*, 2009), the most prominent feature of the present apo CRP structure that was distinct from the cAMP-bound form is the compact dimerization of the CDDs (Leu134–Tyr206), which accomplishes the inward positioning of the F-helices (αFs; Fig. 1*a*). Despite apparent conflicts with the reported NMR structure of apo CRP (Popovych *et al.*, 2009), we conclude that the CDD dimerization of apo CRP would also be relevant in solution (see Supporting Information). The local folds of the two CDDs are nearly identical, and they associate in a twofold symmetry with an antiparallel coiled-coil assembly of the αDs that provides a fundamental dimer interface (Sharma *et al.*, 2009; Fig. 1*b* and Supplementary Fig. S2*a*). Here, we observe for the first time the strong hydrophobic clusters formed at the ends of the coiled coil which stabilize CDD dimerization (Fig. 2*a*). Each hydrophobic core is constructed as a mutual packing of the two CDDs between Leu134 and Leu137 in one subunit and Ala144, Leu147, Leu148, Leu190, Leu195, Ile196 and Val205 in the opposite subunit. The involvement of the αF residue Leu190 in this hydrophobic cluster contributes to constraining the inactive orientation of the DNA-binding αF towards the NND. As similarly discussed by Sharma *et al.* (2009), the increased conformational stability of the D138L-CRP crystal can also be attributed to the supplementation of this hydrophobic cluster with the neighbouring hydrophobic side chain of Leu138 to the innate Leu134 and Leu137 residues (Fig. 2*a*). In particular, Leu134 occupies the core of the cluster, which is surrounded by the other eight hydrophobic side chains. The participation of Leu134 in this hydrophobic cluster appears to be the structural basis that maintains the long αD of apo CRP that begins at Leu134, which forms a backbone hydrogen bond to Asp138. Upon cAMP binding to CRP, the Leu134 side chains are translocated into the newly generated hydrophobic core at the C-termini of the αCs (Fig. 2*b*), which severs the backbone hydrogen bond to Asp138 and results in a newly formed hydrogen bond to Lys130, thereby leading to C-terminal elongation of αC and N-terminal diminution of αD. Similarly, in

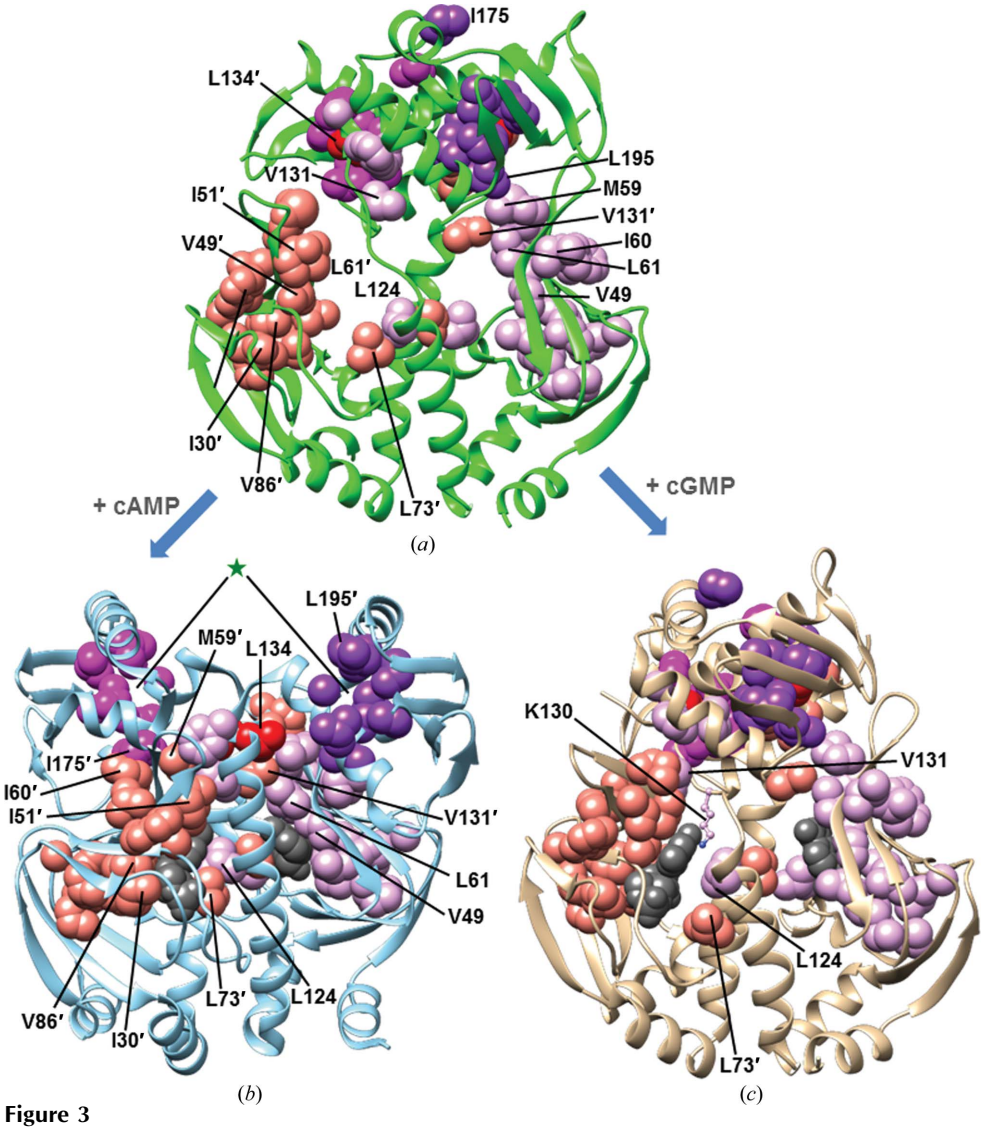

Figure 3
Distribution of the central hydrophobic clusters that differentiate the CRP conformations. Residues in the closed subunit are labelled with primes. Hydrophobic side chains are depicted as spheres and are coloured orchid (NND) and purple (CDD) for the open subunit and salmon (NND) and magenta (CDD) for the closed subunit, with the Leu134 residues coloured red. Ribbon representations of apo CRP (*a*), cAMP–CRP (*b*) and cGMP–CRP (*c*) are coloured green, sky blue and tan, respectively. The bound cAMP (*b*) and cGMP (*c*) molecules are depicted as grey spheres. In the cAMP-bound structure (*b*), the positions formerly occupied by Leu134 in the apo state are indicated with green stars.

the known structure of the CRP-family protein CooA, the conserved leucine (Leu130 in CooA, Leu134 in CRP) has been suggested to occupy the central fulcrum for the conformational change of the hinge conformation (Lanzilotta *et al.*, 2000). Once Leu134 has been ejected, the aforementioned CDD hydrophobic clusters are not integrated (indicated by a star symbol in Fig. 3*b*) and the CDD dimer dissociates. Even at the altered position caused by cAMP binding, the Leu134 residues play a central role in bridging the two hydrophobic clusters of individual NNDs at their C-termini (Fig. 2*b*). Hence, the functional switch of Leu134 appears to be one of the central regulatory machineries in CRP.

3.3. Asymmetry and interdomain interaction of the apo CRP structure

Like the CDDs, the two NNDs (Pro9–Val126) dimerize in a twofold-symmetric manner (Fig. 1*c*). The structural aspects of the NND dimerization are apparently the same as observed in the known CRP structures and are fundamentally mediated by the coiled-coil assembly of the αCs. Despite the symmetric dimerization in the NNDs and CDDs, the overall conformation of the present apo CRP structure is characterized by an overall asymmetry between the subunits; *i.e.* one subunit is in an 'open' conformation with a relatively splayed orientation between the NND and the CDD, whereas the other adopts a 'closed' relatively stooping conformation (Fig. 1*a*). Thus, the appreciable asymmetry is regarded as originating primarily from a different conformation of the interdomain hinge region (Val126–Asn133; see Supporting Information). Owing to the asymmetry in domain orientations, the interdomain interactions are also differently organized between the subunits. For example, the electrostatic interaction between the Glu54 side chain of the closed subunit (E54′ in Fig. 4*a*; henceforth, residues in the closed subunit are denoted with primed numbers) and the Arg185 guanidino group of the open subunit is not relevant between Arg185′ and Glu54. Glu129 is involved in the intersubunit interaction that stabilizes the cNMP-binding site of the opposite subunit by interacting with Arg123′ (Fig. 5*a*), whereas Glu129′ provides an interdomain interaction with Phe188′ in its own subunit (Fig. 4*a*). In addition, the intersubunit interaction between Ser128 and Lys130′ (Fig. 5*a*) is not formed between Ser128′ and Lys130. Likewise, the Gln193 side chain forms a water-mediated indirect hydrogen bond to the backbone of Gly132′ (Fig. 4*a*),

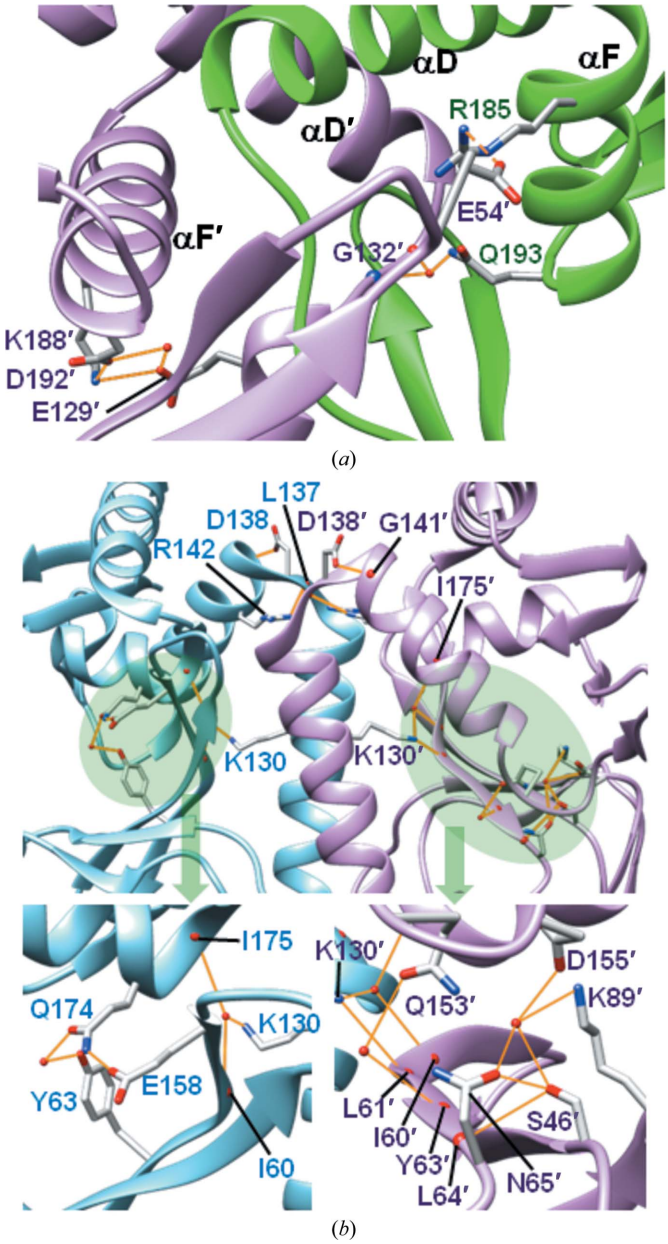

Figure 4
Electrostatic interdomain interactions between the CDD and NND of apo CRP (*a*), cAMP–CRP (*b*) and cGMP–CRP (*c*). Hydrogen bonds and salt bridges are depicted by orange lines. N and O atoms are coloured blue and red, respectively. Water molecules and backbone atoms involved in hydrogen-bonding networks are also depicted as small spheres. The residues in the closed subunits (orchid ribbon) are denoted with primed numbers.

whereas Gly132 and Gln193′ do not interact. The hydrophobic interaction between Met59 and Leu195 (Fig. 3*a*) is also not valid in the closed subunit. Although those interdomain interactions in apo CRP are not comparable in detail to those observed in the cAMP-bound CRP, it is a common aspect that the interactions are predominantly mediated *via* the hinge and the so-called flap (the $\beta4$–$\beta5$ hairpin) regions in the NNDs. However, their interaction counterparts in the CDDs are critically distinguished, *i.e.* αF in apo CRP (Fig. 4*a*) instead of αD and αE in cAMP–CRP (Fig. 4*b*) mainly mediates the interdomain interactions, albeit not abundantly. This inspection suggests that the inward retention of αFs in the dimerized CDD is responsible for the inactivity of apo CRP.

3.4. Crystallization and overall conformation of cGMP–CRP

Despite a homologous structure with the purine moiety and a comparable affinity for CRP binding, cGMP, unlike cAMP,

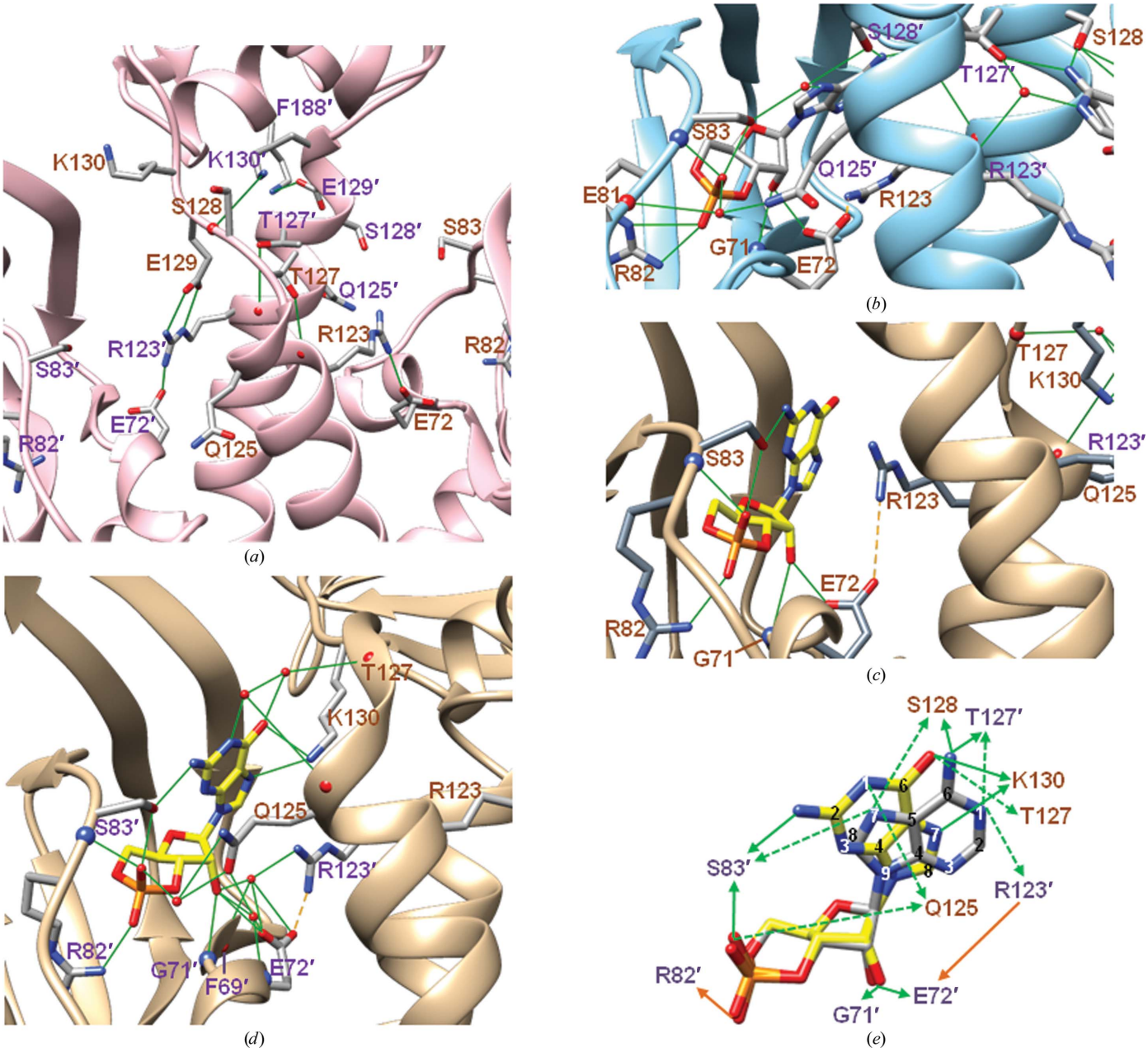

Figure 5
Electrostatic interactions in the cNMP-binding sites. The residues in the closed subunits are denoted with primed numbers. N and O atoms are coloured blue and red, respectively. In apo CRP (*a*) and cAMP–CRP (*b*) and in the open (*c*) and closed (*d*) subunits of the cGMP–CRP structure, hydrogen bonds are depicted as green lines and salt bridges as dashed orange lines. Water molecules and backbone atoms involved in the hydrogen-bonding networks are also depicted as small spheres. (*e*) Comparison of the electrostatic interactions between CRP and the bound *anti* cAMP (grey) with the *syn* cGMP (yellow) in the closed subunit. Direct electrostatic interactions (hydrogen bonds in green and salt bridges in orange) are illustrated by solid arrows, and the water-mediated indirect interactions are depicted as dashed arrows.

cannot induce the activation of CRP. Thus, as a representative cNMP that cannot activate CRP, cGMP is most frequently used as a negative-control probe for investigating CRP allostery. However, cGMP binding to some CRP* mutants (where * indicates a constitutively active phenotype in the absence of cAMP) modulates their activities (Tzeng & Kalodimos, 2012, 2013). Thus, in the present work the cGMP–CRP complex structure was investigated to supplement the insight into the structural basis of the inactive state and to examine the potential role of cGMP in the structural regulation of CRP. For the cGMP–CRP complex, full-length CRP was prepared (Sharma *et al.*, 2009; Won *et al.*, 2002) and crystallized in the presence of cGMP. The crystals contained two dimer molecules in the asymmetric unit with no significant differences in their determined conformations. Therefore, the dimer molecule that was designated as chains *A* and *B* was selected for structural interpretation in this paper. The overall topology of the cGMP-bound CRP structure closely resembles the apo CRP structure, with an apparent intersubunit asymmetry of relatively open and closed forms (Fig. 1*a*).

We have previously revealed that a CRP dimer maximally binds two molecules of cGMP, whereas four cAMP molecules can bind to the CRP dimer in solution (Won *et al.*, 2002). Binding of two *anti* cAMPs at the NNDs results in a conformational change of CRP that generates two additional binding sites for *syn* cAMPs at the CDDs (Małecki *et al.*, 2000; Won *et al.*, 2002; Scott & Jarjous, 2005). The *syn* cAMP binding to CRP is assumed to function as feedback inhibition, most likely by interfering with the CRP–DNA interaction (Won *et al.*, 2002). However, *anti* cAMP binding at the NND, which is essential for the functional activation of CRP, was distinguished from the common *syn* cAMP binding in the cAMP-specific PKA and Epac proteins (Sharma *et al.*, 2009; Das *et al.*, 2009). In the present cGMP–CRP structure, the local folds of the cNMP-binding β-rolls are similar to those observed in cAMP–CRP (Fig. 1*c*). However, the electron density clearly identifies the bound cGMP molecules in a *syn* conformation in both subunits (Supplementary Fig. S3 and Fig. 5), which is consistent with previous predictions based on NMR and molecular modelling (Tzeng & Kalodimos, 2013; Weber *et al.*, 1989) but is in contrast to the observed *anti* conformation of cAMP at the equivalent sites (Passner *et al.*, 2000; Weber & Steitz, 1987; Won *et al.*, 2000).

3.5. Stepwise binding and specific recognition of *syn* cGMP

Through a close inspection of the cAMP–CRP structure, Weber & Steitz (1987) supposed that cAMP first binds to the β-roll residues *via* interactions with the phosphoribose, which is followed by adenine interactions. A similar stepwise binding of cAMP has been suggested based on the known crystal structures of the cNNP-binding domains in a PKA and in a cAMP-dependent ion channel, where the latter contact occurs *via* the phosphate (Rehmann *et al.*, 2007). Notably, the present cGMP–CRP structure captured the differential binding of cGMP between the subunits, with tighter binding in the closed subunit with more direct and indirect interactions with CRP than in the open subunit (Fig. 5). This observation is distinguished from the symmetric organization of the two cAMP bindings at equivalent sites which was found in the cAMP–CRP crystal structures (Fig. 5*b*). Because NMR analyses of the cNMP-bound CRP showed no detectable asymmetry of the complex (Won *et al.*, 2000, 2002; Tzeng & Kalodimos, 2013), it is reasonable to suppose that the observed asymmetry of the cGMP binding reflects an intermediate state of the cGMP–

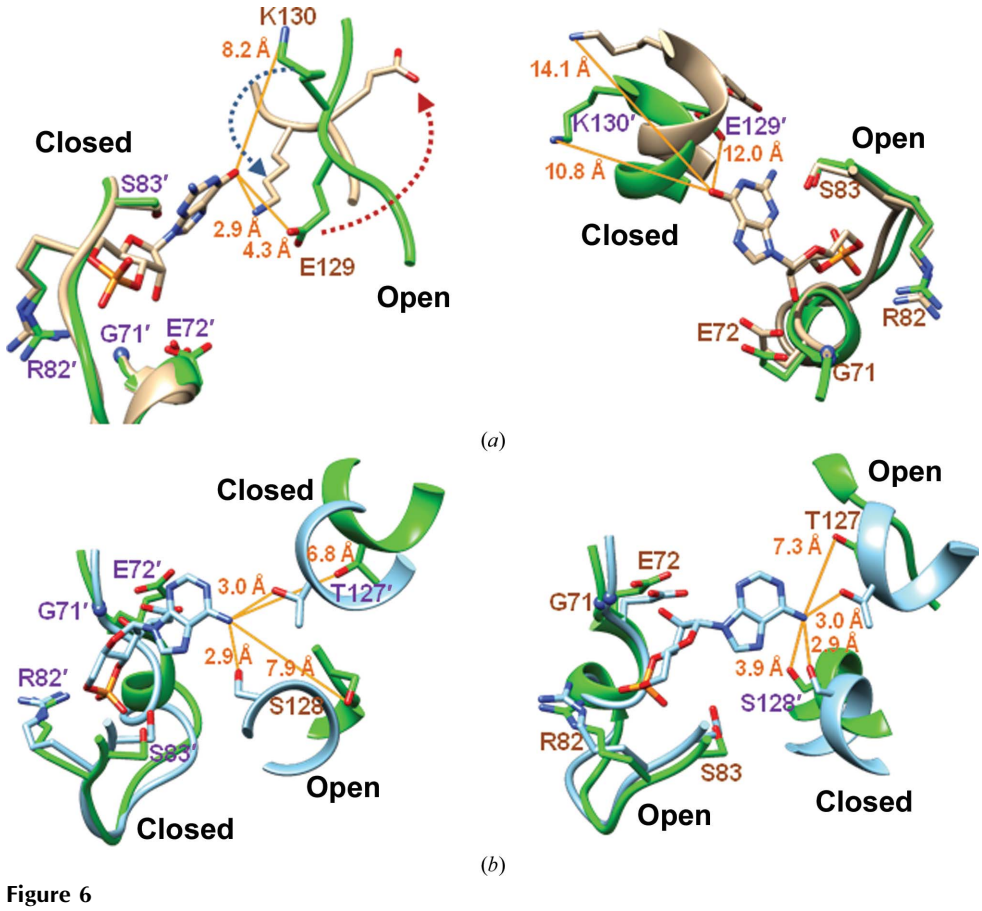

Figure 6
Superposition of cNMP-binding sites of individual subunits in apo CRP and the cNMP–CRP complex. The nascent bindings of cGMP (*a*) and cAMP (*b*) are modelled by superposition of the equivalent C^{α} atoms of Gly71, Glu72, Arg82 and Ser83 in the individual subunits of apo CRP (green), cGMP–CRP (tan) and cAMP–CRP (sky blue). The residues in the closed subunits are labelled with primes.

CRP in which the two subunits might be undergoing a rapid conformational exchange in solution. Thus, given that this crystallographic snapshot reflects an intermediate state and/or a stabilized conformer of the cGMP-bound CRP, it constitutes the first structural evidence for the stepwise mode of cNMP binding which has been conceptually deduced.

The minimal binding mode observed in the open subunit (Fig. 5*c*) is assignable to a nascent binding that accommodates the inbound cNMP onto the floor of the preformed cNMP-binding site of apo CRP (Figs. 5*a* and 6*a*) *via* direct interactions between the common cNMP phosphoribose and the conserved β-roll residues Gly71, Glu72, Arg82 and Ser83 of CRP. The nascent binding also includes common hydrophobic and van der Waals interactions that pack the inbound cNMP onto the preformed β-roll hydrophobic cluster; *i.e.* the top face of the cNMP interacts with the side chains of Leu61 and Val49 *via* the purine ring and with the side chains of Val86 and Ile30 *via* the furanose ring, whereas the bottom face of the furanose ring interacts with Leu73 (Figs. 3*a* and 3*c*; Harman, 2001; Passner *et al.*, 2000; Tomlinson *et al.*, 2006). This initial binding mode is nearly identical for cAMP and cGMP binding, and the electrostatic interactions between the Glu72 and Arg123 side chains are conserved, even in apo CRP (Fig. 5). However, the purine ring-mediated interactions are different between cAMP and cGMP and appear to be the structural determinants for discriminating *syn* and *anti* conformers by specifically stabilizing one of them. In particular, the interaction between Ser83 (the hydroxyl O atom) and the purine ring (the N2 amine of cGMP), which is fully responsible for stabilizing the *syn* conformation of the bound cGMP (Fig. 5*c*), is not possible in either *anti* or *syn* cAMP. When in the *syn* conformation, the N2 amine of the cGMP forms a hydrogen bond to the hydroxyl O atom of Ser83 (Fig. 5*e*). In contrast, the N6 amine of cAMP cannot form the equivalent hydrogen bond owing to its long distance from Ser83, even when it adopts a *syn* conformation. Alternatively, the N3 atom of cAMP, when in the *syn* conformation, can orient towards the proximal Ser83 hydroxyl group for hydrogen bonding. However, because the hydroxyl group of Ser83 acts primarily as a hydrogen donor to the exocyclic phosphate O1 atom, the additional hydrogen bond to the N3 atom cannot be formed. Consequently, the bound cAMP cannot be stabilized in the *syn* conformation by Ser83.

It is important to note that the interaction between the hydroxyl group (Ser83) and guanine ring (cGMP) is involved in the minimal binding mode (Fig. 5*c*), which could enable CRP to selectively recognize the *syn* conformation of cGMP at the nascent binding step. However, to our knowledge, no conserved specific interaction that determines the *syn* or *anti* conformation of the bound cAMP has been identified in cNMP-regulated proteins. As mentioned above, even CRP binds *syn* cAMP at the additionally formed binding sites of the CDDs. The observation of the *syn* and *anti* conformations of cAMP bound to PKG (Kim *et al.*, 2011) also supports the idea that the aforementioned selection mechanics of *syn* or *anti* cNMP during nascent binding could preferentially operate for cGMP. Instead, the hydroxyl O atom of Ser83 in CRP is also likely to stabilize the *anti* conformation of the bound cAMP, as it makes a water-mediated interaction with the N7 atom of the bound *anti* cAMP (Figs. 5*b* and 5*e*). However, this indirect interaction does not appear to be a critical factor for selecting the *anti* conformation of cAMP because it was not evident in the cAMP-bound complex of the CRP orthologue from *M. tuberculosis* (Reddy *et al.*, 2009). Free cAMP molecules in solution have been predicted to slightly favour the *anti* conformation (Altieri *et al.*, 2008). Thus, considering the significant racemization in solution, the initially bound cAMP in CRP is expected to undergo a conformational equilibrium between the *syn* and *anti* conformations before the final settlement, with a slight preference for the *anti* conformer. Then, the settlement of the bound geometry in the *anti* conformation could be accomplished upon later contacts that are mediated by the N6 amino group. The *syn* conformations of cAMPs bound to PKAs are often observed to be stabilized by interactions *via* the N6 amine (Diller *et al.*, 2001). Meanwhile, free cGMP molecules in solution are expected to be heavily biased toward the *syn* conformation (Altieri *et al.*, 2008). Thus, the interaction of Ser83 with guanine may be more significant for the specific binding of cGMP rather than the discrimination between the *syn* and *anti* conformations of cGMP. Indeed, the hydroxyl group is well conserved as a serine or threonine in CRP orthologues and cGMP-dependent PKGs (Supplementary Fig. S4*a*) and is most likely to be important for the specific recognition of cGMP. We also confirmed from the ITC results (Supplementary Fig. S5) that the Ser83 hydroxyl group is crucial for the initial cGMP binding. The cGMP-binding parameters determined for wild-type CRP [$K_a = (3.9 \pm 0.3) \times 10^4\ M^{-1}$, $\Delta H = -2.9 \pm 0.08$ kcal mol^{-1}, $\Delta S = 11.2 \pm 0.0$ cal mol^{-1} K^{-1}] were in good agreement with those previously estimated by Lin & Lee (2002) [$K_a = (4.2 \pm 0.3) \times 10^4\ M^{-1}$, $\Delta H = -2.7 \pm 0.08$ kcal mol^{-1}, $\Delta S = 12.1 \pm 0.0$ cal mol^{-1} K^{-1}]. In contrast, the mutant in which alanine replaced Ser83 (S83A-CRP) showed no appreciable binding to cGMP.

The second step of cNMP binding in CRP includes a tight settlement of the bound cNMP *via* additional indirect interactions that are mediated by water molecules, as observed in the closed subunit of the present cGMP–CRP structure (Fig. 5*d*) and in both subunits of the cAMP–CRP structure (Fig. 5*b*). For example, the water-mediated indirect interaction between the cGMP phosphate in the closed subunit and the Gln125 side chain in the open subunit is consistent with that observed in the cAMP-binding mode (Fig. 5*e*). Concomitant with this stabilization, the purine rings of the cNMPs appear to interact with the C-helices (αCs) and hinge regions of CRP to generate specific structural features, which are distinct between cAMP and cGMP. In particular, the hydrogen-bonding interactions *via* the 6-keto group of cGMP contrast with those of the cAMP N6 amino group (Fig. 5*e*). It has previously been well established that the direct interactions between the cAMP N6 amino group and Thr127 of its own subunit and Ser128 from the neighbouring subunit are critical factors that trigger the allosteric transition of CRP (Won *et al.*, 2009; Harman, 2001). In contrast, the 6-keto group of the

bound *syn* cGMP forms a direct hydrogen bond to Lys130 of the opposite subunit (Fig. 5*d*). The present ITC results support the involvement of this interaction in the second step of cGMP binding (Supplementary Fig. S5). Compared with the wild-type CRP [K_a = (3.9 ± 0.3) × 10^4 M^{-1}, ΔH = −2.9 ± 0.08 kcal mol^{-1}, ΔS = 11.2 ± 0.0 cal mol^{-1} K^{-1}], K130A-CRP exhibited only a modest reduction in cGMP-binding affinity [K_a = (3.4 ± 0.3) × 10^4 M^{-1}, ΔH = −1.2 ± 0.02 kcal mol^{-1}, ΔS = 16.8 ± 0.0 cal mol^{-1} K^{-1}], whereas the S83A mutation almost abolished the cGMP-binding ability of CRP. Since Lys130 upon cGMP binding corresponds to Thr127 and Ser128 upon cAMP binding, the tight binding of cGMP to K130A-CRP is consistent with the previous observations that amino-acid substitutions at positions Thr127 and Ser128 showed no remarkable effect on the initial cAMP binding, although they were critical for mediating the allosteric transition (Harman, 2001). As well as the Lys130 interaction, two water-mediated interactions with CRP that are most likely to stabilize the bound geometry of the guanine ring are also observed for the 6-keto group and the N1 atom of cGMP. These indirect interactions appear to compensate for the water-mediated interactions of the N1 atom of cAMP (Fig. 5*e*).

3.6. Conformational change of CRP on cGMP binding

A close inspection of the cGMP–CRP structure demonstrates that CRP undergoes a certain conformational change upon binding cGMP. The CDD dimer in the cGMP–CRP structure is more tilted and rotated compared with that in apo CRP (Fig. 1*b*). This cGMP-induced CDD rotation is directed, albeit subtly, opposite to that induced by cAMP (Fig. 7) and strengthens the interdomain interactions mediated by the F-helices (αFs) through a greater number of interactions than in apo CRP (Fig. 4*c*). Essential conformational changes to generate the CDD reorientation are observed in NNDs. In particular, the atomic interaction between the 6-keto O atom of cGMP in the closed-subunit cGMP and the Lys130 side chain of the open subunit (Fig. 5*d*) compels the altered conformation of the open-subunit hinge (Fig. 6*a*), which primarily contributes to the reorientation of the CDD dimer.

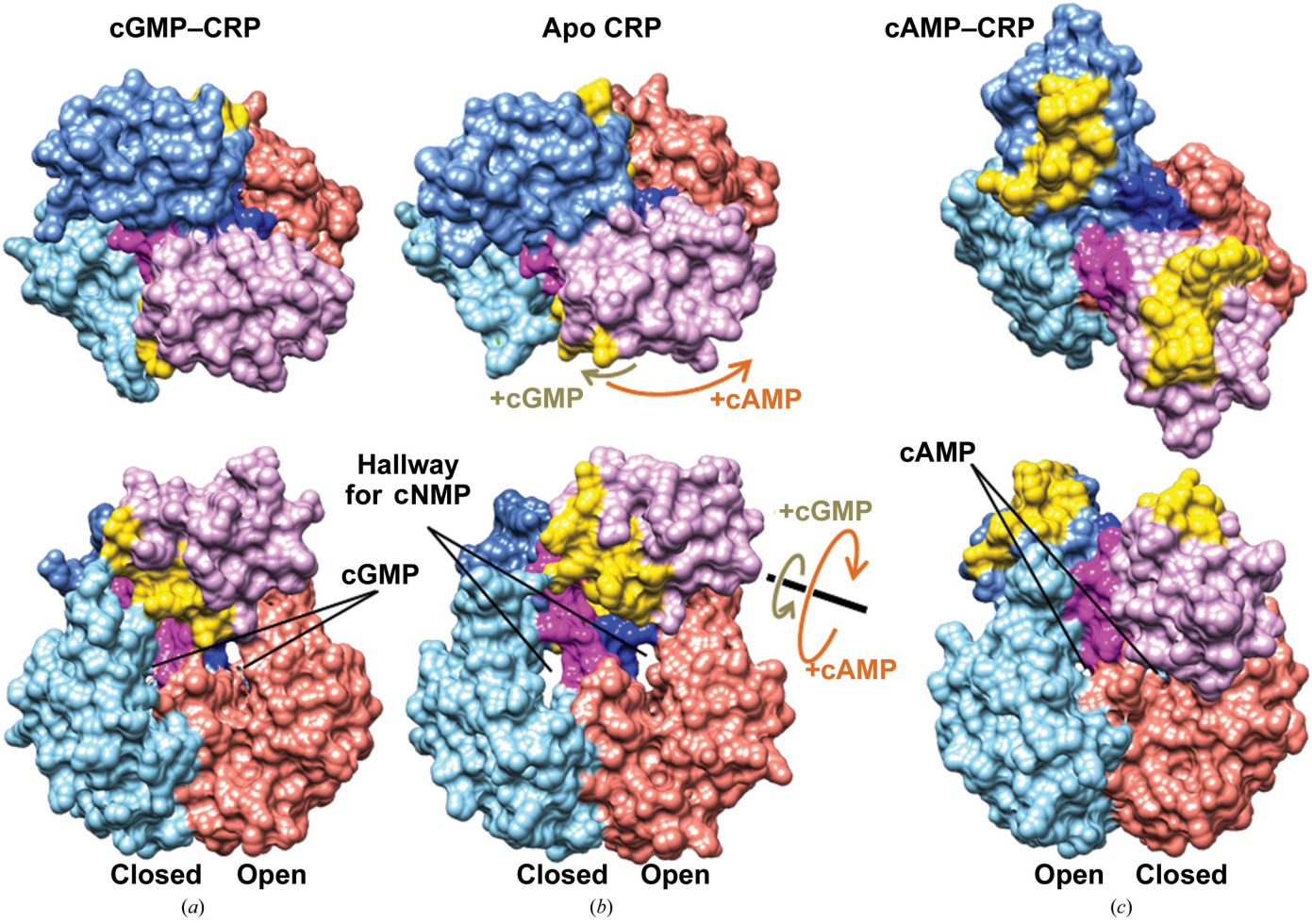

Figure 7
Comparison of the domain orientations of the cGMP–CRP (*a*), apo CRP (*b*) and cAMP–CRP (*c*) structures. The upper and lower panels represent the top and the front view, respectively, of each molecule. Surfaces of the NND, hinge and CDD are coloured salmon, magenta and orchid, respectively, in the open subunit and sky blue, blue and cornflower blue, respectively, in the closed subunit. The DNA-recognizing αFs in both subunits are indicated in gold. Directions of the cNMP-induced CDD rotations are indicated by arrows on the apo CRP structure (*b*).

In addition, the slightly altered hinge conformation results in flipping of the Glu129 side chain (Fig. 6*a*), which formerly interacted with Arg123 of the opposite subunit in apo CRP (Fig. 5*a*), to centrally mediate the intersubunit and interdomain interactions in cGMP–CRP (Fig. 4*c*).

It has also been well established that the flap stretches (the $\beta4$–$\beta5$ hairpin region in Fig. 1*a*) crucially mediate the allosteric conformational change of CRP. Upon cAMP binding, the complete flaps move towards the hinge by more than 10 Å (Fig. 1*c*), resulting in contraction of the NNDs, which has also been demonstrated biochemically (Won *et al.*, 2009; Harman, 2001; Passner *et al.*, 2000). In particular, the Lys130 residue also plays an important role in maintaining the altered flap position in the cAMP–CRP structure (Fig. 4*b*). In contrast, the shortened distance between the flaps is not relevant in the cGMP–CRP structure (Fig. 1*c*), where the Lys130 side chain of the open subunit interacts with the bound cGMP in the closed subunit (Fig. 5*d*). However, superposition of the NNDs indicates that a subtle inward motion of the flap occurred in the open subunit, whereas it laterally swung out in the closed subunit (Fig. 1*c* and Supplementary Fig. S2*b*). Because the flap residues are involved in the interdomain interactions with the residues from the αF helix in the CDD (Fig. 4*c*), the subtle reorientation of the CDD dimer in cGMP–CRP is attributable to the flap repositioning in concert with the hinge alteration.

Another significant change upon cGMP binding is verified in the cNMP-binding site. In apo CRP, the Leu73 and Leu124 pairs form a small hydrophobic cluster (Fig. 3*a*). In the open subunit of cGMP–CRP, which reflects the mode of nascent binding, the Leu73 side chain interacts with the bottom face of the furanose ring of the bound cGMP, while its preformed hydrophobic interaction with Leu124 of the opposite subunit in CRP was weakened (Fig. 3*c*). In addition, in the closed subunit of cGMP–CRP, which represents complete binding of cGMP, including the second-step binding, the interaction of Leu73 with Leu124 of the opposite subunit was disrupted and the bound cGMP was compelled to not pack onto Leu73 (Fig. 3*c*). In contrast, the hydrophobic Leu73–Leu124 cluster is retained in the cAMP–CRP structure (Fig. 3*b*). Furthermore, the bound cAMP is compactly stacked onto the cluster *via* hydrophobic interactions with the Leu73 and Leu124 residues. In particular, the interaction between the purine ring of cAMP and the Leu124 side chain of the opposite subunit (Fig. 3*b*), which is not formed in cGMP binding (Fig. 3*c*), can be regarded as a second-step interaction that is specific to cAMP binding. This interaction has also been suggested to be important for the cAMP-induced allosteric transition of CRP; *i.e.* a long-range signal transmission that bypasses αC begins from Leu124 and reaches the hinge residue Lys130 through cAMP and Leu61 (Harman, 2001; Tomlinson *et al.*, 2006). Thus, during cGMP binding the presence of an atomic interaction with the Lys130 side chain and the absence of the Leu124 interaction appear to be inhibitory factors that prevent the allosteric activation of CRP.

Collectively, the structural consequences of cGMP binding appear to be inhibitory to CRP, rather than null, as they are accomplished by specific and stepwise interactions with the Ser83 and Lys130 residues. This potential for cGMP to inhibit CRP could also be relevant to the complete deactivation of a dynamically activated T127L/S128I-CRP* mutant by cGMP binding (Tzeng & Kalodimos, 2013; see §4 for details).

4. Discussion

4.1. Conformational allostery of CRP by cAMP and cGMP binding

The paucity and controversy of high-resolution atomic structures of inactive CRP species have precluded a definite elucidation of CRP allostery. The present apo CRP and cGMP–CRP structures commonly corroborate that the inward positioning of the DNA-recognizing αFs *via* CDD dimerization is the primary structural determinant of their functional inactivity, while the conformational transition by cAMP is apparently accomplished through dissociation and rigid-body rotation of the two CDDs (Figs. 3 and 7). The fact that the substitution of a hydrophobic residue in the CDD dimer interface, such as Ala144, Leu148 or Leu195, shown in Fig. 2, by a polar amino acid results in a constitutively active CRP* phenotype (Won *et al.*, 2009; Harman, 2001; Passner *et al.*, 2000) also indicates that CDD dissociation would be the most critical requirement for CRP activation.

The present structures provide macroscopic and microscopic insights into the mechanism of the global conformational transition of CRP. Firstly, cAMP binding results in a conformational change in CRP that can be described as a central convergence of hydrophobic clusters (Fig. 3*b*) which were formerly distributed to the αCs, flaps (the $\beta4$–$\beta5$ hairpins) and CDDs in the apo form (Fig. 3*a*), accompanied by a helical adoption of the central hinge region (Val126–Asn133; Supplementary Fig. S1*b*). Thus, this conformational change appears to simply follow the fundamental driving forces of protein folding in solution to construct a hydrophobic core through internal convergence of hydrophobic side chains with neutralization of main-chain polarity *via* hydrogen bonds to form secondary structures. Owing to the vacancy of the cNMP-binding sites in apo CRP, the overall optimization of the hydrophobic core includes the compact CDD dimerization (Fig. 3*a*). However, upon the compact packing of cAMP, the spontaneous reconstitution of the optimal hydrophobic core (Fig. 3*b*) results in dissociation and a rigid-body rotation (Fig. 7) of the CDDs without an alteration in their innate folds (Supplementary Fig. S2*a*), which leads to protrusion of the αFs in order to be compatible with DNA binding. The atomic details of these conformational changes are described below and validate the previous identification of crucial residues for the allosteric transition (Won *et al.*, 2009; Harman, 2001; Passner *et al.*, 2000; Tomlinson *et al.*, 2006).

During nascent binding, the inbound cAMPs are fitted into the preformed binding sites of the β-rolls *via* electrostatic interactions with the Gly71, Glu72, Arg82 and Ser83 residues (Fig. 5*c*) and hydrophobic stacking onto the Ile30, Val86, Val49, Leu61 and Leu73 residues (Fig. 3*c*). Additional interactions, as the second step of binding, then accomplish the

conformational change. At the beginning of this transition, the Leu124 residues in the αCs, which interact with the Leu73 residues (Fig. 3*a*), tug the initially bound cAMPs *via* a hydrophobic interaction force to stack the purine ring (bottom face) onto the αC helix (Fig. 3*b*). Thus, the β-rolls that were adhered to the cAMPs are also forced to move, resulting in contraction of the NNDs through an inward motion of the flaps towards the hinge by more than 10 Å (Fig. 1*c* and Supplementary Fig. S2*b*). The bound cAMPs then shift towards the αCs and establish hydrogen bonds with the hinge (the N6 amine of cAMP with Thr127 of the corresponding subunit and Ser128 of the opposite CRP subunit; Figs. 2*b*, 5*b* and 6*b*), whereas the flap residue Leu61 that interacted with cAMP forms an additional interaction with the hinge residue Lys130 (Fig. 4*b*; Tomlinson *et al.*, 2006). Because the hinge in apo CRP is dynamic in nature and demonstrates an inherent helical propensity (see Supporting Information), the reduced flexibility through the immobilization of Thr127, Ser128 and Lys130 results in a firm stabilization of the helical conformation through a reconstitution of their backbone hydrogen-bonding networks, such as those between Arg123, Thr127 and Val131, between Leu124, Ser128 and Gly132 and between Val126, Lys130 and Leu134 (Supplementary Fig. S1*b*). As the hydrophobic clusters at the flaps are repositioned near the hinge, the helix formation at the hinge is further forced to neutralize the main-chain polarity and to gather the nearby small hydrophobic clusters that are composed of the side chains of Leu134, Ala135, Phe136 and Leu137 (Figs. 2 and 3). Thus, the propagating hydrogen-bonding networks beginning at the N-proximal region of the hinge finally reach the Leu137 amide proton and end between Leu137 and Asp138, which results in C-terminal elongation of αC (Popovych *et al.*, 2009; Won *et al.*, 2000) and N-terminal diminution of αD (Sharma *et al.*, 2009; Tzeng & Kalodimos, 2013). Thus, the Leu137 and Asp138 residues constitute a new short hinge that connects the CDDs and NNDs (Fig. 4*b*), and the CDD dimer, which is deprived of Leu134 and Leu137 at the critical dimer interface, dissociates into monomers (Figs. 2 and 3). Concomitantly, the concerted hydrogen-bonding forces at the hinge are translated to a helical torque that triggers a rigid-body rotation of the dissociated CDDs. Finally, the altered orientations of the CDDs are stabilized *via* the αDs and αEs that interact with the new hinges and the repositioned flaps (Fig. 4*b*).

All of the atomic momentum driving the cAMP-induced global transition of CRP can operate in a concerted manner and can be completely blocked by cGMP, which renders CRP inert by inducing an opposite conformational change to that induced by cAMP. In particular, the 6-keto group of the bound cGMP directly hydrogen bonds to Lys130 of the hinge in the opposite subunit (Figs. 3*a* and 5*d*), which rivets the hinge as an extended stretch that does not fold into a helix (Fig. 6*a*) and prevents the aforementioned long-range signal transmission bypassing the αC helix (from Leu124 to Lys130 through Leu61 in cAMP binding; Tomlinson *et al.*, 2006). It is noteworthy that Lys130, which is crucial for the signal translation of cAMP binding and conformational transition of CRP, was specifically grabbed by cGMP to avoid conformational activation. Additionally, as the Lys130 interaction thrusts out the bound cGMP (Fig. 3*c*), the flap laterally swings out (Fig. 1*c* and Supplementary Fig. S2*b*). The outward motion of the β-roll detaches the cGMP from Leu73 and furthermore disrupts the preformed Leu73–Leu124 interaction (Fig. 3*c*) that otherwise functions as the aforementioned beginning of the transition to the active state. Finally, the altered conformation of the hinge and the shifted position of the flap detain the αFs more strongly than in apo CRP (Fig. 4*c*), which results in a further deactivation of CRP.

4.2. Interpretation of the dynamic allostery of CRP

In terms of protein dynamics, allosteric transitions are often described as an equilibrium shift of the pre-existing active-state and inactive-state populations based on a conformational selection theory of stabilization of the active state by the allosteric effector (Tzeng & Kalodimos, 2009, 2012, 2013). However, in the active conformation of CRP the entrance for the effector to approach the binding pocket is blocked (Fig. 7*c*) owing to the inward positioning of the flaps (Fig. 1*c*). Previously, this observation by Weber & Steitz (1987) led to the concept of a certain conformational change after cAMP binding. Because the active conformation is not likely to be selected for cAMP binding, owing to the closure of the entrance, it is difficult to imagine that apo CRP is under such an equilibrium. Thus, it is supposed that the conformational allostery primarily operates and is then combined with dynamic allostery that affects the internal dynamics (Popovych *et al.*, 2006). Indeed, recent NMR-based dynamics approaches have indicated neither the active-state population of apo CRP nor the inactive-state population of cAMP–CRP for the wild-type protein, whereas the active–inactive equilibrium was valid in some CRP* mutants (Tzeng & Kalodimos, 2009, 2012, 2013). Our model for conformational change also successfully explains the dynamic allostery of CRP* mutants coupled with cNMP effects as follows.

A dynamically activated T127L/S128I-CRP* is completely deactivated by cGMP binding (Tzeng & Kalodimos, 2013), whereas the population dynamics of the A144T-CRP* mutant are not perturbed (Tzeng & Kalodimos, 2012). The observed equilibrium between inactive (93%) and active (7%) populations of the T127L/S128I-CRP* mutant are attributable to the aforementioned functional switch of Leu134 (Fig. 2*b*). Substitution of Thr127 and Ser128 by hydrophobic residues efficiently leads to the formation of a hydrophobic cluster at the hinge (Tzeng & Kalodimos, 2013; Youn *et al.*, 2006; Chu *et al.*, 2001). Therefore, it is highly probable that the newly formed hydrophobic cluster produces pressure that tugs the neighbouring small hydrophobic clusters in the flaps and in the αDs (the Leu134-Ala135-Phe136-Leu137 cluster) to construct an optimized central hydrophobic core (Fig. 3*b*). It is also known that the double mutation increases the helical propensity of the hinge region (Won *et al.*, 2009; Tzeng & Kalodimos, 2013; Youn *et al.*, 2006; Chu *et al.*, 2001). Helical adoption by the hinge would further facilitate tugging Leu134 from the CDD dimer by shortening the distance to this residue

and forming a backbone hydrogen bond to Lys130 (Fig. 2*b*). All of these potential forces for structural conversion closely resemble the effects of cAMP binding but would be relatively weaker than the forces produced by the compact packing of cAMP in wild-type CRP. Consequently, only a small population of the active state, which can hardly be detected by NMR, can be equilibrated. Subsequent cGMP binding to the mutant prevents all of the flap movements, the helical adoption of the hinge and the Leu134 functional switch, thereby abolishing the active-state population. Meanwhile, the observed half-population of the active state that is generated in the A144T-CRP* mutant is attributable to the weakened hydrophobic core in the CDD dimer (Fig. 2*a*), which can induce its dissociation without the aid of the allosteric effect from the NND. Thus, cGMP binding at the NND will not inhibit the innate population of active CDDs in the A144T-CRP* mutant. Instead, the bound cGMP affects the protein dynamics to enhance its DNA-binding affinity *via* increased conformational entropy (Tzeng & Kalodimos, 2012; Baldwin & Kay, 2012).

In contrast to wild-type CRP, the S62F-CRP mutant undergoes dynamic exchange of inactive and active populations in its cAMP-bound state, and this equilibrium was found to be biased toward the inactive form (98%; Tzeng & Kalodimos, 2009). Substitution of Ser62, which is located near the bound cAMP (Fig. 2*b*), by a bulky hydrophobic phenylalanine residue could sterically hinder or modify the compact packing of cAMP. In particular, an NMR study of this mutant revealed cAMP-induced resonance shifts for Val49, Leu61, Leu73 and Leu124, which differed from those observed for cAMP binding to wild-type CRP (Harman, 2001; Lee *et al.*, 1991). This finding implies that the cNMP-binding site occupied by cAMP in the S62F mutant would resemble that occupied by cGMP in wild-type CRP, particularly for the binding of the phosphoribose moiety, as shown in Fig. 3(*c*). Thus, the incomplete binding geometry of cAMP in this mutant is insufficient to induce an active population, although it can still activate the protein *via* enhanced conformational entropy for DNA binding (Tzeng & Kalodimos, 2012; Baldwin & Kay, 2012).

Collectively, a thorough understanding of protein allostery can be achieved with integrated insight into the conformational and dynamic allostery. In particular, the conformational aspects of the allosteric transition are inevitably helpful for an enlightened understanding of the dynamic allostery. In this respect, the present results establish a model for such an integrative insight into protein allostery.

4.3. Interpretation of the sequential binding of cNMPs

Because CRP contains two identical cNMP-binding sites in a dimer, the cooperativity in cNMP binding has been interpreted as a sequential binding mode comprised of two binding steps. In particular, the interpretation of the observed cooperativity in cAMP binding has been a challenge (Won *et al.*, 2009; Tutar, 2008; Scott & Jarjous, 2005; Małecki *et al.*, 2000) since the identification of additional cAMP-specific binding sites at the CDDs, which are formed after complete occupancy of the N-terminal cNMP-binding sites by cAMPs (Won *et al.*, 2002; Scott & Jarjous, 2005). Indeed, a triphasic binding response and negative and positive cooperativity have been detected for cAMP (Won *et al.*, 2009; Lin & Lee, 2002; Tutar, 2008). However, a dynamics study on an isolated NND dimer clearly demonstrated negative cooperativity in the sequential binding of two cAMPs at the N-terminal cNMP-binding sites (Popovych *et al.*, 2006). The observed asymmetry between the subunits of the present structures establishes a working model for the sequential binding of cNMPs that discriminates between cAMP and cGMP, as follows (Fig. 8).

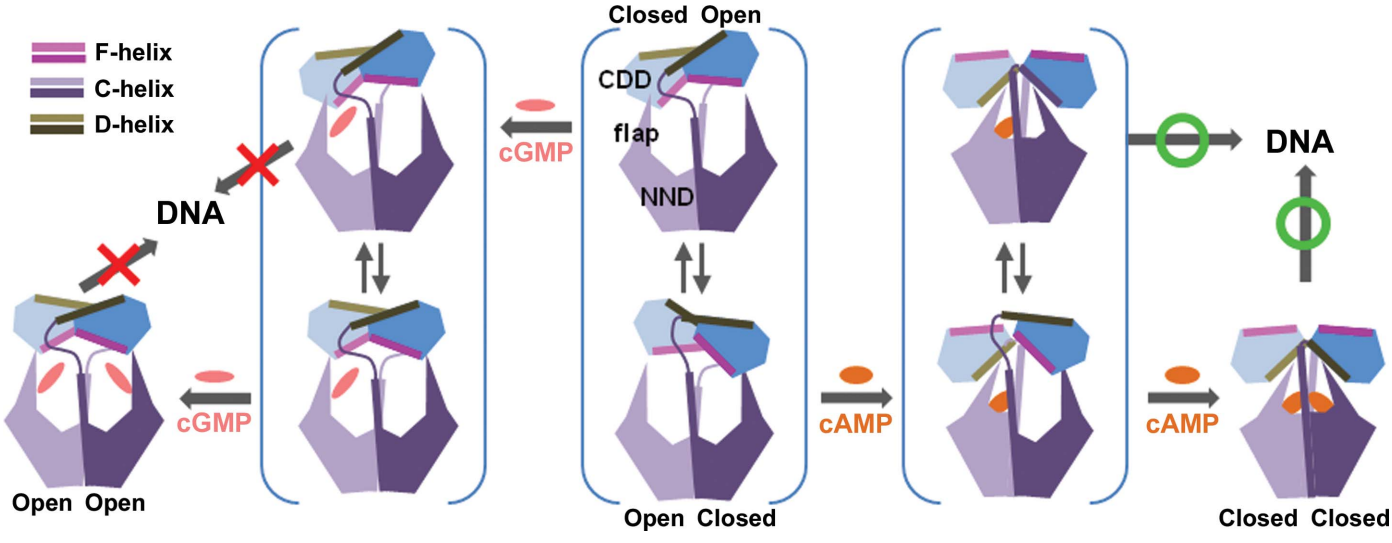

Figure 8
Model for the discriminatory structural regulation of CRP by sequential binding of cAMP and cGMP. Conformational exchanges are indicated by antiparallel arrow pairs. The change in αC and αD lengths, the inward motion of the flaps, the closure of the entrance for cAMP and the dissociation and rotations of the CDDs are illustrated (refer to the main text for a detailed description).

Firstly, the present apo CRP structure suggests a different order of sequential binding to the individual subunits for cAMP and cGMP. Specifically, the aforementioned conformational asymmetry of apo CRP can generate different binding preferences of individual subunits for the first cNMP binding (Fig. 6). Owing to the dynamic nature of the hinge region, each subunit of apo CRP in solution is expected to undergo conformational exchange between its open and closed forms, while maintaining symmetric CDD dimerization (see Supporting Information). Thus, given that this asymmetry could be relevant, even if transiently, in the nascent cNMP-binding step, subsequent interaction between the cGMP that is bound at the open subunit with the Lys130 of the closed subunit would not be favoured owing to the reverse direction of the Lys130 side chain (Figs. 5*a* and 6*a*, right). Conversely, the side chain of Lys130 in the open subunit faces toward the cGMP at the closed subunit to readily interact with it with only a minor change in the hinge geometry (Figs. 5*a* and 6*a*, left). The preformed close proximity (approximately 4.3 Å) between the 6-ketone of cGMP and the negatively charged side chain of Glu129 (Fig. 6*a* left) may facilitate the hinge conversion by inducing a repulsion that flips the side chain of Glu129. In sharp contrast to cGMP binding, complete binding of cAMP is preferred at the open subunit. The positions of both hinges in apo CRP relative to the nascent cNMP-binding site in the open subunit are already similar to those observed in the cAMP–CRP structure (Fig. 6*b*, right), whereas these positions deviate when compared with the nascent cNMP-binding site in the closed subunit (Fig. 6*b*, left). Additionally, upon the nascent binding of cAMP to the open subunit, the side chain of Ser128 in the closed subunit is expected to be in particularly close proximity (approximately 3.9 Å) for preferential binding (Fig. 6*b*, right), whereas the side chain of Ser128 in the open subunit is oriented away from the cAMP-binding site of the closed subunit (Figs. 5*a* and 6*b*, left). This observation additionally suggests that the Ser128 interaction may be involved in the nascent binding of cAMP, thereby contributing to the selective stabilization of the *anti* conformation of the initially bound cAMP.

In summary, for complete binding of the first cNMP at the NND, it is suggested that cAMP is preferred in the open subunit, whereas cGMP is preferred in the closed subunit. Then, owing to these different preferences, the cNMP-binding site in the closed subunit is first firmly occupied by cGMP and fixes the opposite subunit in an open state through the interaction with Lys130, whereas the closed subunit remains able to exchange between open and closed states (Fig. 8, middle left). When the first cGMP-bound subunit is in the open state, the second cGMP that is bound at the opposite subunit interacts with its hinge to also stabilize the open state (Fig. 8, left). Finally, both subunits are stabilized in an open state that is not compatible with DNA binding owing to the inward immobilization of the αFs. In contrast, the cNMP-binding site in the open subunit of apo CRP is preferred for the binding of the first cAMP (Fig. 8, middle right). The subsequent settlement of the bound cAMP is accomplished *via* the inward motion of the flap and a helical elongation of the hinge, as previously described, which results in the dissociation and rotation of the CDD of the open subunit. The interaction of the cAMP of the open subunit with Ser128 of the closed subunit, which is already present within a helix (Supplementary Fig. S1*b*), may not be sufficient to induce the further helical elongation that is required for the rotation of the CDD of the closed subunit. However, the cAMP-free subunit can now undergo a conformational exchange between the open and closed flap conformations (Fig. 8, middle right), which would be favoured for the optimization of the central hydrophobic core, leading to rotation of the CDD *via* elongation of αC and diminution of αD. These dynamics can underlie the entropy-driven CRP allostery that was previously observed (Popovych *et al.*, 2006; Tzeng & Kalodimos, 2012), *i.e.* a dynamic conformational exchange is implicit in the considerable motional flexibility, particularly on the microsecond to millisecond time scale, of the cAMP-free NND once the opposite site is occupied by cAMP (Popovych *et al.*, 2006). Subsequently, the state induced by the conformational exchange is nearly identical to the final structure occupied by two cAMPs and is highly compatible with DNA binding (Fig. 8, right). This model addresses the puzzling finding that one molar equivalent of bound cAMP per CRP dimer is sufficient for activation of the protein (Won *et al.*, 2009; Harman, 2001; Tutar, 2008). Moreover, this active conformation with one cAMP can only rarely recruit the second cAMP because the entrance is closed (Fig. 7*c*) by the inward repositioning of the flap. Thus, the conformational exchange in the singly occupied cAMP-bound state can operate as an adverse factor for subsequent cAMP binding, which underlies the known negative cooperativity of the first cAMP binding that interferes with subsequent cAMP binding at the NNDs (Won *et al.*, 2009; Harman, 2001; Popovych *et al.*, 2006).

4.4. Molecular-evolutionary implications of cNMP discrimination

The present results revealed that the conserved Ser83 residue of CRP is critical for the specific recognition of cGMP in a *syn* conformation at its nascent binding step (Fig. 5*c*). Because residues such as serine, threonine and alanine can be readily substituted with one another by a single-point mutation at the first base of the corresponding codon (Weber *et al.*, 1989), all of the cNMP-regulated proteins appear to contain one of these residues at the conserved position (Supplementary Fig. S4*a*; Rehmann *et al.*, 2007; Weber *et al.*, 1098; Altieri *et al.*, 2008; Kumar & Weber, 1992; Altenhofen *et al.*, 1991). Among these residues, serine and threonine, both of which possess a hydroxyl group that is able to act as both a hydrogen-bond donor and a hydrogen-bond acceptor, are responsible for the specific binding of *syn* cGMP and are therefore highly conserved in the cGMP-dependent protein kinases (PKGs) and in the recently identified cGMP-binding domain of a cyclic di-GMP synthase (An *et al.*, 2013). Moreover, the cNMP-regulated ion channels, including a majority of cAMP-dependent channels, contain a conserved threonine or serine. In contrast, all of the PKAs and Epac proteins

contain an alanine at the equivalent position as a proton donor *via* its backbone amide. Substitution of the conserved alanine with threonine in a PKA specifically increased its cGMP-binding affinity (Kumar & Weber, 1992; Shabb *et al.*, 1990). Conversely, the threonine-to-alanine mutation in cNMP-regulated ion channels resulted in a dramatic decrease in cGMP sensitivity, and a threonine-to-serine mutation even improved the cGMP sensitivity (Altenhofen *et al.*, 1991). In this context, highly intriguing questions are raised, such as why the cAMP-specific CRP contains serine for the specific recognition of cGMP and why this residue is not conserved in cAMP-specific PKAs but is conserved in cGMP-specific PKGs. Because the functional consequence of cGMP, if practically involved in bacterial signalling, would be the opposite of that of cAMP (Bernlohr *et al.*, 1974), discrimination between cGMP and cAMP may be essential for CRP for an exhaustive control of cAMP signalling, even if cGMP is simply a byproduct of adenylate cyclase, as has long been argued (Gomelsky, 2011; Linder, 2010). In particular, the 6-keto group of cGMP, if in an *anti* conformation, possesses sufficient potential to act as a hydrogen-bond acceptor to form hydrogen bonds to the Thr127 and Ser128 side chains to trigger allosteric activation of CRP (Weber *et al.*, 1989). Thus, it is possible that CRP has developed a clever system to discriminate cNMPs prior to structural conversion, and the mechanics that discriminate the false cGMP ligand may have evolved into PKGs to specifically recognize the *syn* cGMP as their *bona fide* effector. Alternatively, the specific recognition of cGMP appears to be somewhat redundant for CRP because the mutation of serine to alanine, as in PKAs and Epac proteins, could simply avoid binding of cGMP by quenching its binding affinity. Moreover, because the *syn* conformation already predominates over the *anti* conformation for free cGMP in solution (Altieri *et al.*, 2008), the aforementioned undesirable effect by a potential *anti* cGMP would be negligible. Thus, the interaction of Ser83 with guanine may be more significant for specific binding of cGMP rather than for its discrimination (Kumar & Weber, 1992). In this respect, the present structure also opens the intriguing possibility that cGMP in prokaryotes has been underappreciated, with doubtful evidence on the absence of cGMP signalling in *E. coli* (Gomelsky, 2011). Recently, cGMP has been demonstrated to be a *bona fide* second messenger in other bacteria (Gomelsky, 2011; Gomelsky & Galperin, 2013; Marden *et al.*, 2011; An *et al.*, 2013) and the evolutionary relationships between cAMP and cGMP have been preferentially implemented in bacterial genes encoding nucleotidyl cyclases and CRP homologues (Gomelsky, 2011; An *et al.*, 2013). In this context, the possibility that the as yet unidentified bacterial cGMP signalling may be mediated by CRP-like proteins cannot be excluded (Gomelsky, 2011; An *et al.*, 2013). Additionally, some CRP-family proteins, such as PrfA (Eiting *et al.*, 2005), SdrP (Agari *et al.*, 2008) and TTHB099 (Agari *et al.*, 2012), of which the apo forms closely resemble the cAMP-bound CRP conformation, exert an inherent activity without effector molecules. Hence, the present observation that the bound cGMP aggressively exerted an inhibitory effect on the CRP structure, rather than a null effect, additionally suggests that a specific inhibition of the global transcription factor CRP may be involved in the bacterial cGMP signalling pathway. In eukaryotes, *syn* cGMP is an agonist of *syn* cAMP that activates cAMP-dependent PKAs (Das *et al.*, 2009). However, *anti* cGMP is recognized by the Epac proteins that are also selectively activated by *syn* cAMP and elicits antagonism by modulating the entropic control of inhibitory interactions (Das *et al.*, 2009). Thus, conversely, the functional antagonism of *syn* cGMP in the CRP systems that utilize *anti* cAMP might be relevant in prokaryotes. Finally, it is strongly suggested that the cGMP signalling universe in prokaryotes is worthy of a thorough examination, in parallel to further structural studies on the cGMP-bound forms of other cAMP-regulated proteins.

4.5. Related literature

The following references are cited in the Supporting Information for this article: Borjigin *et al.* (2007), Joyce *et al.* (2006), Komori *et al.* (2007) and Mills & Dean (1996).

The authors thank S. J. Lee (College of Pharmacy, Chungbuk National University) for helpful discussion on the crystallization and the staff at beamline NW12A of the Photon Factory, Japan for their assistance during X-ray data collection. This work was supported by the Pohang Accelerator Laboratory (PAL) through the abroad beam time program of the Synchrotron Radiation Facility Project under MEST and was performed under the approval of the Photon Factory Program Advisory Committee (Proposal No. 2011G237). This work was also supported by the National Research Foundation of Korea (NRF; grants 20070056817, 2012R1A2A1A01003569, NRF-2009352-E00041 and 20110013663) funded by the Korean Government, the Korea Healthcare Technology R&D Project, Ministry for Health, Welfare and Family Affairs, Republic of Korea (A092006) and the 2012 BK21 Project for Medicine, Dentistry and Pharmacy.

References

Adams, P. D., Grosse-Kunstleve, R. W., Hung, L.-W., Ioerger, T. R., McCoy, A. J., Moriarty, N. W., Read, R. J., Sacchettini, J. C., Sauter, N. K. & Terwilliger, T. C. (2002). *Acta Cryst.* D**58**, 1948–1954.
Agari, Y., Kashihara, A., Yokoyama, S., Kuramitsu, S. & Shinkai, A. (2008). *Mol. Microbiol.* **70**, 60–75.
Agari, Y., Kuramitsu, S. & Shinkai, A. (2012). *Proteins*, **80**, 1490–1494.
Altenhofen, W., Ludwig, J., Eismann, E., Kraus, W., Bönigk, W. & Kaupp, U. B. (1991). *Proc. Natl Acad. Sci. USA*, **88**, 9868–9872.
Altieri, S. L., Clayton, G. M., Silverman, W. R., Olivares, A. O., De la Cruz, E. M., Thomas, L. R. & Morais-Cabral, J. H. (2008). *J. Mol. Biol.* **381**, 655–669.
An, S.-Q., Chin, K.-H., Febrer, M., McCarthy, Y., Yang, J.-G., Liu, C.-L., Swarbreck, D., Rogers, J., Dow, J. M., Chou, S.-H. & Ryan, R. P. (2013). *EMBO J.* **32**, 2430–2438.
Baldwin, A. J. & Kay, L. E. (2012). *Nature (London)*, **488**, 165–166.
Berman, H. M., Ten Eyck, L. F., Goodsell, D. S., Haste, N. M., Kornev, A. & Taylor, S. S. (2005). *Proc. Natl Acad. Sci. USA*, **102**, 45–50.
Bernlohr, R. W., Haddox, M. K. & Goldberg, N. D. (1974). *J. Biol. Chem.* **249**, 4329–4331.
Borjigin, M., Li, H., Lanz, N. D., Kerby, R. L., Roberts, G. P. & Poulos, T. L. (2007). *Acta Cryst.* D**63**, 282–287.
Botsford, J. L. & Harman, J. G. (1992). *Microbiol. Rev.* **56**, 100–122.

Brünger, A. T. (1992). *Nature (London)*, **355**, 472–475.
Chan, M. K. (2000). *Nature Struct. Biol.* **7**, 822–824.
Chen, V. B., Arendall, W. B., Headd, J. J., Keedy, D. A., Immormino, R. M., Kapral, G. J., Murray, L. W., Richardson, J. S. & Richardson, D. C. (2010). *Acta Cryst.* D**66**, 12–21.
Chu, S. Y., Tordova, M., Gilliland, G. L., Gorshkova, I., Shi, Y., Wang, S. & Schwarz, F. P. (2001). *J. Biol. Chem.* **276**, 11230–11236.
Clayton, G. M., Silverman, W. R., Heginbotham, L. & Morais-Cabral, J. H. (2004). *Cell*, **119**, 615–627.
Das, R., Chowdhury, S., Mazhab-Jafari, M. T., Sildas, S., Selvaratnam, R. & Melacini, G. (2009). *J. Biol. Chem.* **284**, 23682–23696.
Diller, T. C., Madhusudan, Xuong, N.-H. & Taylor, S. S. (2001). *Structure*, **9**, 73–82.
Eiting, M., Hagelüken, G., Schubert, W. D. & Heinz, D. W. (2005). *Mol. Microbiol.* **56**, 433–446.
Emsley, P., Lohkamp, B., Scott, W. G. & Cowtan, K. (2010). *Acta Cryst.* D**66**, 486–501.
Gallagher, D. T., Smith, N., Kim, S.-K., Robinson, H. & Reddy, P. T. (2009). *J. Biol. Chem.* **284**, 8228–8232.
Gomelsky, M. (2011). *Mol. Microbiol.* **79**, 562–565.
Gomelsky, M. & Galperin, M. Y. (2013). *EMBO J.* **32**, 2421–2423.
Harman, J. G. (2001). *Biochim. Biophys. Acta*, **1547**, 1–17.
Hollands, K., Busby, S. J. W. & Lloyd, G. S. (2007). *FEMS Microbiol. Lett.* **274**, 89–94.
Joyce, M. G., Levy, C., Gábor, K., Pop, S. M., Biehl, B. D., Doukov, T. I., Ryter, J. M., Mazon, H., Smidt, H., van den Heuvel, R. H., Ragsdale, S. W., van der Oost, J. & Leys, D. (2006). *J. Biol. Chem.* **281**, 28318–28325.
Kabsch, W. & Sander, C. (1983). *Biopolymers*, **22**, 2577–2637.
Kim, J. J., Casteel, D. E., Huang, G., Kwon, T. H., Ren, R. K., Zwart, P., Headd, J. J., Brown, N. G., Chow, D.-C., Palzkill, T. & Kim, C. (2011). *PLoS One*, **6**, e18413.
Kleywegt, G. J. & Jones, T. A. (1998). *Acta Cryst.* D**54**, 1119–1131.
Komori, H., Inagaki, S., Yoshioka, S., Aono, S. & Higuchi, Y. (2007). *J. Mol. Biol.* **367**, 864–871.
Kumar, P., Joshi, D. C., Akif, M., Akhter, Y., Hasnain, S. E. & Mande, S. C. (2010). *Biophys. J.* **98**, 305–314.
Kumar, V. D. & Weber, I. T. (1992). *Biochemistry*, **31**, 4643–4649.
Lanzilotta, W. N., Schuller, D. J., Thorsteinsson, M. V., Kerby, R. L., Roberts, G. P. & Poulos, T. L. (2000). *Nature Struct. Biol.* **7**, 876–880.
Lee, B. J., Aiba, H. & Kyogoku, Y. (1991). *Biochemistry*, **30**, 9047–9054.
Lin, S.-H. & Lee, J. C. (2002). *Biochemistry*, **41**, 11857–11867.
Linder, J. U. (2010). *Mol. Cell. Biochem.* **334**, 215–219.
Małecki, J., Polit, A. & Wasylewski, Z. (2000). *J. Biol. Chem.* **275**, 8480–8486.
Marden, J. N., Dong, Q., Roychowdhury, S., Berleman, J. E. & Bauer, C. E. (2011). *Mol. Microbiol.* **79**, 600–615.
Matthews, B. W. (1968). *J. Mol. Biol.* **33**, 491–497.
Mills, J. E. & Dean, P. M. (1996). *J. Comput. Aided Mol. Des.* **10**, 607–622.
Murshudov, G. N., Skubák, P., Lebedev, A. A., Pannu, N. S., Steiner, R. A., Nicholls, R. A., Winn, M. D., Long, F. & Vagin, A. A. (2011). *Acta Cryst.* D**67**, 355–367.
Otwinowski, Z. & Minor, W. (1997). *Methods Enzymol.* **276**, 307–326.
Passner, J. M., Schultz, S. C. & Steitz, T. A. (2000). *J. Mol. Biol.* **304**, 847–859.
Pettersen, E. F., Goddard, T. D., Huang, C. C., Couch, G. S., Greenblatt, D. M., Meng, E. C. & Ferrin, T. E. (2004). *J. Comput. Chem.* **25**, 1605–1612.
Popovych, N., Sun, S., Ebright, R. H. & Kalodimos, C. G. (2006). *Nature Struct. Mol. Biol.* **13**, 831–838.
Popovych, N., Tzeng, S.-R., Tonelli, M., Ebright, R. H. & Kalodimos, C. G. (2009). *Proc. Natl Acad. Sci. USA*, **106**, 6927–6932.
Puljung, M. C. & Zagotta, W. N. (2013). *J. Biol. Chem.* **288**, 12944–12956.
Reddy, M. C., Palaninathan, S. K., Bruning, J. B., Thurman, C., Smith, D. & Sacchettini, J. C. (2009). *J. Biol. Chem.* **284**, 36581–36591.
Rehmann, H., Wittinghofer, A. & Bos, J. L. (2007). *Nature Rev. Mol. Cell Biol.* **8**, 63–73.
Schünke, S., Stoldt, M., Lecher, J., Kaupp, U. B. & Willbold, D. (2011). *Proc. Natl Acad. Sci. USA*, **108**, 6121–6126.
Schüttelkopf, A. W. & van Aalten, D. M. F. (2004). *Acta Cryst.* D**60**, 1355–1363.
Scott, S. P. & Jarjous, S. (2005). *Biochemistry*, **44**, 8730–8748.
Shabb, J. B., Ng, L. & Corbin, J. D. (1990). *J. Biol. Chem.* **27**, 16031–16034.
Sharma, H., Yu, S., Kong, J., Wang, J. & Steitz, T. A. (2009). *Proc. Natl Acad. Sci. USA*, **106**, 16604–16609.
Tomlinson, S. R., Tutar, Y. & Harman, J. G. (2006). *Biochemistry*, **45**, 13438–13446.
Tutar, Y. (2008). *Cell Biochem. Funct.* **26**, 399–405.
Tzeng, S.-R. & Kalodimos, C. G. (2009). *Nature (London)*, **462**, 368–372.
Tzeng, S.-R. & Kalodimos, C. G. (2012). *Nature (London)*, **488**, 236–240.
Tzeng, S.-R. & Kalodimos, C. G. (2013). *Nature Chem. Biol.* **9**, 462–465.
Van Duyne, G. D., Standaert, R. F., Karplus, P. A., Schreiber, S. L. & Clardy, J. (1993). *J. Mol. Biol.* **229**, 105–124.
Weber, I. T., Shabb, J. B. & Corbin, J. D. (1989). *Biochemistry*, **28**, 6122–6127.
Weber, I. T. & Steitz, T. A. (1987). *J. Mol. Biol.* **198**, 311–326.
Winn, M. D. *et al.* (2011). *Acta Cryst.* D**67**, 235–242.
Won, H.-S., Lee, Y.-S., Lee, S.-H. & Lee, B.-J. (2009). *Biochim. Biophys. Acta*, **1794**, 1299–1308.
Won, H.-S., Lee, T.-W., Park, S.-H. & Lee, B.-J. (2002). *J. Biol. Chem.* **277**, 11450–11455.
Won, H.-S., Yamazaki, T., Lee, T.-W., Yoon, M.-K., Park, S.-H., Kyogoku, Y. & Lee, B.-J. (2000). *Biochemistry*, **39**, 13953–13962.
You, C., Okano, H., Hui, S., Zhang, Z., Kim, M., Gunderson, C. W., Wang, Y.-P., Lenz, P., Yan, D. & Hwa, T. (2013). *Nature (London)*, **500**, 301–306.
Youn, H., Kerby, R. L., Conrad, M. & Roberts, G. P. (2006). *J. Biol. Chem.* **281**, 1119–1127.
Zagotta, W. N., Olivier, N. B., Black, K. D., Young, E. C., Olson, R. & Gouaux, E. (2003). *Nature (London)*, **425**, 200–205.
Zhang, P., Smith-Nguyen, E. V., Keshwani, M. M., Deal, M. S., Kornev, A. P. & Taylor, S. S. (2012). *Science*, **335**, 712–716.